Supplementary Information

Unraveling Electrochemical Glycine Conversion Pathways for Ammonia Recovery from Organic Waste

Haldrian Iriawan[+*1], Jedidian Adjei[+2], Danae A. Haro Chipoco[+3], Dayana Donneys Victoria[4], Asa Ashley,[5] Andrew J. Medford[*6], Marta C. Hatzell[*7], Gerardine G. Botte[*4], Yang Shao-Horn[*1,5,8]

[1]Department of Materials Science & Engineering, Massachusetts Institute of Technology, Cambridge, MA, 02139, United States

[2]Department of Chemical Engineering, Texas Tech University, Lubbock, TX 79409

[3]School of Materials Science and Engineering, Georgia Institute of Technology, Atlanta, GA, 30332, USA

[4]Institute for Sustainability Circular Economy, Texas Tech University, Lubbock, TX 79409

[5]Research Laboratory of Electronics, Massachusetts Institute of Technology, Cambridge, MA, 02139, United states

[6]School of Chemical & Biomolecular Engineering, Georgia Institute of Technology, Atlanta, GA, 30332, United States

[7]George W. Woodruff School of Mechanical Engineering, Georgia Institute of Technology, 770 Ferst Ave, Atlanta, GA, 30309, USA

[8]Department of Mechanical Engineering, Massachusetts Institute of Technology, Cambridge, MA, 02139, United States

[+]Equally contributing authors

[*]Corresponding authors

Table of contents

Materials

Nickel foil electrodes (0.25 mm thick, annealed, 99.5% metal basis, Thermo Scientific), anion exchange membrane (DSVN, thickness = 95 μm, Bellex International Corp.), KOH (semiconductor grade, 99.99% trace metals basis, Sigma Aldrich), Glycine (≥ 99%, Sigma Aldrich), Ag/AgCl reference electrode, Hg/HgO reference electrode, Pt mesh (99.99%, StonyLab), Ar (99,999%, Airgas or Linde), deionized water (18.2 MΩ cm, Millipore), ammonium standards (99.999% NH_4Cl, VeriSpec®), $^{13}C_2$ glycine (99 atom% ^{13}C, Sigma), 2% HNO_3 (ICP grade, Sigma), Ethanol (Sigma), Ortho-phosphoric acid (H_3PO_4, Sigma) Other materials are specified in the main text and the extended experimental section.

Extended experimental section

Indophenol blue method for NH_4^+ quantification. Three solutions were used: (i) coloring solution, (ii) oxidation solution, and (iii) oxidation solution. The coloring solution is 1M NaOH, 5 wt% salicylic acid, and 5 wt% sodium citrate. The oxidation solution is 0.05M $NaClO_4$, and the catalyst solution is 1 wt% sodium nitroferricyanide. The sample was prepared by mixing 1mL of the sample was with 1mL of coloring solution, 0.5mL of oxidation solution and 0.1mL of catalyst solution. After 2 hours, the mix was measured using ultraviolet-visible (UV-vis) spectrophotometer (Avantes AvaLight-DHC Ava Spec-3648). The intensity recorded was at 655nm.

Ion-chromatography (Institution 2). Ammonium measurements were conducted using a Dionex Aquion Cation IC system (Thermo Fisher Scientific Inc., CA, USA), also equipped with a Dionex AS-AP autosampler. The system utilized a Dionex CDRS 600 4 mm suppressor and a Dionex Integrion Conductivity Detector CD. Separation was carried out using a Dionex IonPac CS16 analytical column (5 × 250 mm) with a Dionex IonPac CG16 RFIC™ guard column (5 × 50 mm). Calibration and data processing were performed using Chromeleon™ Version 7.2. A VeriSpec® N ammonium standard (as NH4+-N, 1000 ppm in H2O; Cat. No. RV010902500N, Lot 840201E, 99.999% NH4+Cl) was used to prepare the calibration solutions. The method was conducted at 30°C, using 30 mM methanesulfonic acid as the eluent.

Chemical oxygen demand measurements. The sample was diluted 5 times to be within the detection range of the HACH kit. 2.5mL of the diluted sample were introduced into the culture tubes containing the digestion and catalyst solution. The tubes were placed in the block digester at 150°C and heated for 2 hours. After the tubes were cooled in air, the visible absorption of the samples was measured using ultraviolet-visible (UV-vis) spectrophotometer (Avantes AvaLight-DHC AvaSpec-3648). The absorbance evaluated for the quantification was 655nm.

HPLC. High-performance liquid chromatography for carbon products quantification. The system used was Quaternary Solvent Manager-R paired with sample manager FTN-R (Waters). The column used for separation was HPX-87H organic acid analysis column (AMINEX) paired with

Biorad. The detection method was UV-vis at 260nm (2489 UV/Vis Detector, Waters). The eluent was 5mM H_2SO_4, the column flow rate was 0.4mL/min and the column temperature was 30°C.

Ion chromatography (IC) for Nitrogen species and carbon products quantification (Institution 3). All anion measurements were performed using a Dionex Integrion HPICTM RFICTM Anion ion chromatograph (Thermo Fisher Scientific Inc., CA, USA) equipped with a Dionex AS-AP autosampler. The IC system included a suppressor ADRS 600 4mm (Dionex) and an Integrion Conductivity Detector CD (Dionex). Separation was achieved using the anion-exchange column (Dionex): IonPac AS18 RFICTM analytical column (250 mm × 4 mm) coupled with a Dionex IonPac AG18 RFICTM (50 mm × 4 mm). Data acquisition, calibration curve generation, and peak integration were conducted using the Chromeleon software package, Version 7.2. All the reagents used were of analytical grade. Calibration standards were prepared using TraceCERT® standards from Sigma-Aldrich: glycolate (Cat. No. 07391), Formate (Cat. No. 44293), acetate (Cat. No. 51791), oxalate (Cat. No. 73139). Glyoxylic acid monohydrate 98% (ThermoScientific Cat No. 120170250, Lot A0458731) was used for calibration as a reference material. Standard solutions were prepared in a matrix of 0.01M KOH and 0.01M glycine solution. A gradient elution method was used for separation: Acetate and glycolate were analyzed at 50°C with the following elution profile: –6 to 14 minutes: 2 mM KOH; 14 to 25 minutes: linear gradient from 2 mM to 22 mM KOH. Formate, glyoxylic acid, and oxalate were analyzed at 30°C with the following elution profile: –6 to 10 minutes: 20 mM KOH; 10 to 12 minutes: linear gradient from 20 mM to 40 mM KOH. Final concentrations of the analytes ranged from 0.01 to 7 mg/L, depending on the specific compound. Dionex Seven Anion Standard (Cat. No. 057590, Lot 23-87JKS) was used for nitrate and nitrite analysis. Standards were prepared in deionized water and analyzed under the same conditions used for formate, glyoxylic acid, and oxalate. In all the anion analyses, 25 µL of sample of standard solution was injected into the eluent stream. The flow rate was maintained at 1.0 mL/min under gradient elution.

Ammonium measurements were conducted using a Dionex Aquion Cation IC system (Thermo Fisher Scientific Inc., CA, USA), also equipped with a Dionex AS-AP autosampler. The system utilized a Dionex CDRS 600 4 mm suppressor and a Dionex Integrion Conductivity Detector CD. Separation was carried out using a Dionex IonPac CS16 analytical column (5 × 250 mm) with a Dionex IonPac CG16 RFIC™ guard column (5 × 50 mm). Calibration and data processing were performed using Chromeleon™ Version 7.2. A VeriSpec® N ammonium standard (as NH_4^+-N, 1000 ppm in H_2O; Cat. No. RV010902500N, Lot 840201E, 99.999% NH_4^+Cl) was used to prepare the calibration solutions. The method was conducted at 30°C, using 30 mM methanesulfonic acid as the eluent.

Acid digestion and Agilent ICP-OES 5800 Analysis (Institution 3). A 5 mL aliquot was subjected to microwave-assisted digestion using a Milestone Ethos up with SK-15 eT rotor. Following EPA Method 3015A, the sample was treated with 9 mL of HNO_3, 3 mL of HCl, and 1 mL of H_2O_2. The digestion protocol employed a temperature ramp from room temperature to 180°C with a dwell time of 10 minutes, followed by a 20-minute cooling period. Upon completion

of the temperature profile, samples were allowed to cool and equilibrate overnight to ensure complete gas evolution before retrieval. The retrieved sample was further diluted with 2% Nitric acid (Trace metal grade) in a 50 mL metal-free centrifuge tube. Further dilutions were made to ensure the concentrations fall within the standards for calibration 100 ppb to 100 ppm.

Conditions for Inductively coupled Plasma- Optical Emission Spectroscopy ICP-OES measurement are as follows: All measurements were conducted in duplicates, with instrumental parameters configured as follows: pump speed was maintained at 12 rpm, with axial viewing mode selected and a viewing height of 0 mm. The uptake delay and rinse time were established at 25 s. The read time was set to 20 s. Gas flow parameters were set with nebulizer flow at 0.7 L/min, plasma flow at 0.7 L/min, auxiliary flow at 1 L/min, and makeup flow at 0 L/min. The RF power was maintained at 1.45 kW, and a stabilization time of 5 s was employed for each measurement.

Ni metal dissolutions were measured in the ICP at wavelengths of 227.021 nm and 231.604 nm with results averaged to ensure analytical accuracy.

Cyanide Measurement (Institution 3). Cyanide (CN^-) was measured with pyridine barbituric acid method with Cyanide TNTplus Vial Test from HACH®. The HACH DR6000 UV-Vis Spectrophotometer with pre-programmed calibration for HACH TNT 862 Cyanide kits (0.01 – 0.6 mg/L) was used for analysis. Samples were diluted 2 to 5x to ensure they fell within the calibration limit of the instrument.

Supplementary Note 1 – Shared experimental protocol

The following protocol was co-developed, refined shared across the three institutions for generating the benchmarking results in Figure 1.

Making electrolytes

1. Dissolve 2.805 g KOH pellets (sigma) into 500 mL DI water (Millipore) to make 0.1M KOH
2. Dissolve 375.35 mg Glycine (Sigma) into 50 mL 0.1M KOH (Millipore) to make 0.1M Glycine solution in 0.1M KOH -> pH is measured to be between 10.6 - 10.8 using a pH meter

Preparing Ni electrode:

1. Cut 0.5 cm x 1.5 cm of Ni foil and make a wedge to indicate 0.5 cm x 1 cm area.
2. Fill in Orthophosphoric acid (commercial, 85%) sufficiently in a small beaker. Solution will need to be replaced after ~5x polishing
3. Cut a sufficiently sized Ti foil (larger than 2x2 cm^2) for electropolishing
4. Use cable and negative tweezers to position Ni foil WE and Ti foil CE appropriately in a 2 electrode setup
5. Perform Chronoamperometry for 5 minutes at 3 V vs CE, ensuring accuracy of the potential on the screen. Steady state current should be around ~25-30 mA
6. Take out the Ni electrode and wipe with an ethanol-drenched Chemwipe until H_3PO_4 has been removed.
7. Sonicate the Ni electrode in an ethanol-containing beaker for >10 minutes.
8. Replace gloves and dry the Ni electrode overnight (12 h) or longer in a 60 ^oC oven

Preparing H cell:

1. (around once a week) Boil the H- cell in water, and then dry in the 60 ^oC oven overnight.
2. For more regular preparation, rinse the H-cell thoroughly with DI water (at least 5x rinsing), with the anion exchange membrane still installed.
3. For storage, keep H-cell filled with DI water and openings closed – membrane should constantly be in wet condition

Performing Glycine oxidation:

1. Fill both working electrode and counter electrode compartments with 0.1 M Glycine + 0.1M KOH solution
2. Open the Ar gas and bubble the working electrode compartment at 20 sccm for at least 20 mins. Ensure the gas flow is set using the Omega mass flow controller for consistent bubbling during experiments
3. Measure 10 mL of 0.1M HCl trap and ensure the 20 sccm is coming out of the H-cell and that it provides a stable bubble in the acid trap.
4. Assemble Ni foil electrode into the working electrode holder, a small tube for gas, Ag/AgCl or Hg/HgO for reference and Pt mesh or Pt plate for counter. Ensure the position of the working electrode is closest to the membrane to, and counter electrode positioned as close to the membrane as possible, to minimize ohmic resistance. Normally, the solution resistance is between 20-30 Ohm (in the 0.1 M KOH + 0.1 M Glycine)
5. Ensure the small magnetic stirrer is inside – rotate at 300 rpm
6. Turn on electrochemistry, with the following programs:
    a. OCV, 30 s

b. PEIS or GEIS or ZIR* to check solution resistance
c. CV, 50 mV s^{-1}, for current-voltage characterization (usually less than 10 cycles)
d. CA at different potentials, typically 15 mins hold followed by ~5 min OCV for elyte sampling.
e. PEIS or GEIS
f. Final OCV

*note: iR compensation is done manually in all experiments. If running ZIR, make sure it is run as a single program (not followed by the CV or CA programs) or the relevant options are unticked so that no auto-compensation is triggered.

7. In between CA programs (including after initial CV), 3 mL of the 0.1M KOH + 0.1M Glycine electrolyte is sampled using a syringe. The 3 mL is then replaced with a fresh electrolyte solution. Correspondingly, HCl trap solution is also sampled for 1 mL at each sampling point.

<u>RHE calibration:</u>

- Method 1 – indirect calibration with 0.1M KOH electrolyte
  - Pt RDE rotated at 1600 rpm working electrode, Pt wire counter electrode, Ag/AgCl reference electrode.
  - Pt RDE undergoes extensive polishing with a diamond suspension of grid size 0.1 um
  - H_2 bubbling of 0.1M KOH electrolyte for 20 min
  - Record OCV – value should stabilize over 5 mins and record the value
  - Record CV at 50 mV s^{-1} of the HER-HOR region, where the current is maintained lower than <-3 mA to prevent bubble formation. The average of the potential-intercept from forward and backward sweeps at zero current should be in close agreement (<10 mV) to the OCV value
  - The RHE value for 0.1M Glycine + 0.1M KOH is then done by subtracting the RHE value for 0.1M KOH by the Nernstian shift from the pH change with and without glycine.
- Method 2 – direct calibration with 0.1M KOH + 0.1M Glycine electrolyte
  - Identical steps as above, but using 0.1M KOH + 0.1M Glycine electrolyte instead.
  - Note: the HER/HOR CV of the Pt will experience significant decays over time (likely due to glycine poisoning), so the RHE value from CV should be taken based on the 1st CV.
  - Method 1 and method 2 have shown excellent quantitative agreement within 8 mV when considering the 1st CV cycle in glycine containing electrolyte. See Supplementary Note 2 for surface poisoning issues by glycine.

Supplementary Note 2: Ensuring robust RHE conversion in the amino acid--containing electrolyte

RHE conversion is necessary to enable consistent and meaningful interpretation of electrochemical data on a thermodynamic scale. Conventionally, based on oxygen and hydrogen electrocatalysis literature,[1] a robust RHE calibration of the reference electrode is done by performing HER and HOR on Platinum in the electrolyte of interest, where the zero-current intercept averaged between the forward and backward scans indicates the potential with respect to the reference electrode at which 0 V_{RHE} is achieved. For example, such methodology conducted in 0.1 M KOH (pH = 12.8 ± 0.1 with a pH meter) with an Ag/AgCl (sat. KCl) reference electrode, which is used for the electrochemical glycine oxidation experiment, yielded a zero intercept of -0.948 V (**Figure S1a**). This value is consistent with the RHE conversion via solution pH using the equation below (eq. 1-2):

$$V_{RHE} = V_{meas} + 0.197\ V\ (Ag/AgCl,\ sat.\ KCl) + 0.059 * pH \quad (1)$$

$$V_{meas} = V_{RHE} - 0.197\ V\ (Ag/AgCl,\ sat.\ KCl) - 0.059 * pH \quad (2)$$

Where 0 V_{RHE} would equal to the measured potential (V_{meas}) of $0 - 0.197 - 0.059 * (12.8 \pm 0.1) = -0.952\ V \pm 0.006$. Moreover, it is noted that the cyclic voltammetry is stable over 10 cycles (**Figure S1a**). All of these observations indicate the cleanliness of the setup and indicates genuine H_2/OH^- equilibrium is achieved.

When the same methodology is used in the glycine solution (0.1 M KOH +0.1 M glycine), The zero intercept from the first cycle was found to be -0.832 V. This value appears to be consistent with the value obtained from RHE conversion via solution pH: using eq. 2 again, 0 V_{RHE} would correspond to the measured potential (V_{meas}) of $0 - 0.197 - 0.059 * (10.7 \pm 0.1) = -0.828\ V \pm 0.006$. However, this zero intercept was observed to significantly shift, with ~50 mV shifted over 10 cycles. Furthermore, the H_2 evolution currents decayed with cycle number. These observations may be attributed to surface poisoning of Pt by glycine, which is consistent with prior reports showing strong glycine chemisorption[2,3] and can therefore influence the Pt surface quality in establishing HER/HOR equilibrium. Therefore, for the cross-institution benchmarking, the solution pH method of RHE conversion (as discussed in the main text) has been used to improve reproducibility. The same method of RHE conversion has been applied when testing other amino acids, where the solution pH values are 10.7 ± 0.1 for 0.1 M KOH + 0.1 M Alanine, 11.6 ± 0.1 for 0.1 M KOH + 0.1 M Lysine and 10.4 ± 0.1 for 0.1 M KOH + 0.05 M Aspartic acid.

Supplementary Note 3: Reliability issues in Ni dissolution quantification

Throughout the cross-institution benchmarking effort, we encountered issues in reliably quantifying Ni^{2+} dissolution in the post-electrolysis samples. This issue is illustrated in **Figure S24**, where the concentrations and quantity (in umol) of Ni^{2+} quantified within a week of electrolysis showed wide variations despite highly consistent ammonia production and efficiency. Furthermore, there does not appear to be a correlation between the umol of ammonia produced and the measured Ni^{2+} in the electrolyte, suggesting that the issue likely derives from the uncertainty in the quantification itself. Preliminary investigation by Institution 3 (**Figure S25**) showed that one major factor may come from the length of storage, where the same samples with high Ni^{2+} concentration measured 5 months after showed significant decrease in. This loss of Ni^{2+} over time might be due to precipitation of Ni^{2+} in alkaline conditions in the form of hydroxides which may stick to the wall and therefore not sampled upon pipetting (**Figure S25**). Different types of sample treatment such as acid digestion (see experimental method for protocol), acid dilution with the ICP-grade 2% HNO_3, or water dilution did not appear to influence the Ni^{2+} quantification when they were done within a week of the electrolysis. Therefore, for the purpose of presenting the realities of electrochemical glycine oxidation in **Figure 1**, data corresponding to experiments for which Ni^{2+} quantification was done close to the time of electrolysis was presented. We note that despite the large variations in dissolved Ni^{2+} during electrolysis in 0.1 M KOH + 0.1 M glycine electrolyte, these quantities significantly exceed the Ni^{2+} dissolution in the glycine-absent electrolyte (0.1 M KOH), hence pointing at the enhanced Ni instability in the presence of glycine and analogously liganding amino acids.

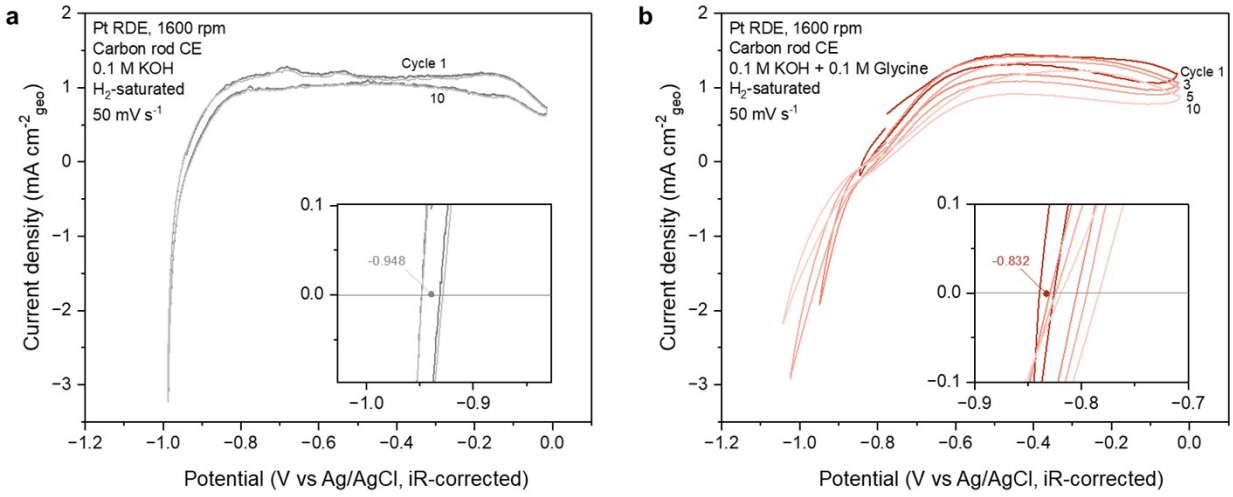

Figure S1. Reference electrode calibration. a-b) Cyclic voltammetry curves of Platinum rotating disk electrode (5 mm diameter, 0.196 cm^2_{geo}) in H_2-saturated 0.1 M KOH (a) and 0.1 M KOH + 0.1 M Glycine (b). The inset shows the 1st cycle zero intercept of the potential, calculated by averaging the potential intercepts from the forward and backward scans.

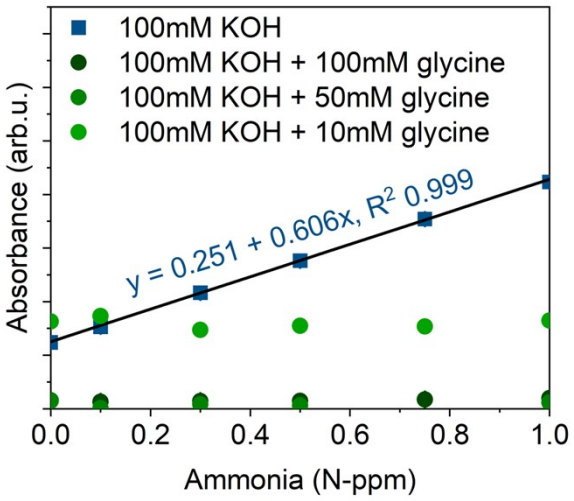

Figure S2. Indophenol blue method for ammonia quantification. NH_3 calibration curve using indophenol blue method in 0.1 M of KOH of electrolyte and 100 mM and 50 mM of glycine present. Indophenol blue method for NH_3 detection does not show characteristic blue color and the associated absorbance when glycine is present.

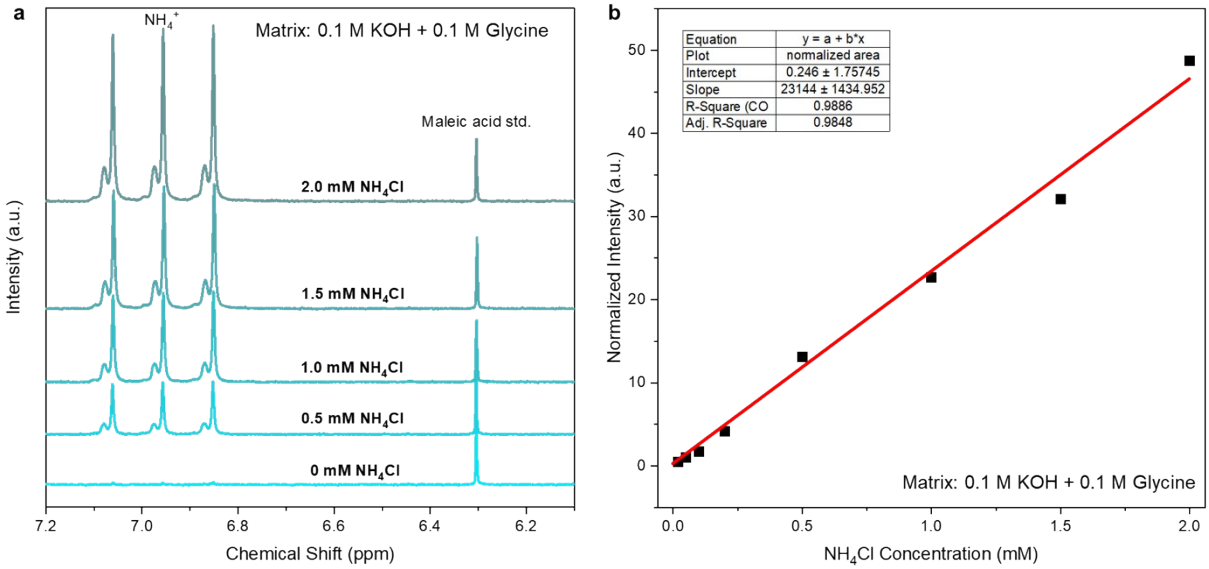

Figure S3. NH_4^+ calibration via H-NMR used for ammonia quantification by Institution 1. a) Representative H-NMR spectra of the NH_4Cl calibration solutions, showing the triplet NH_4^+ peaks between 6.8 - 7.2 ppm and the maleic acid standard at 6.3 ppm. b) Calibration curve showing the NH_4^+ area integration between 6.8 - 7.2 ppm relative to the maleic acid standard (referred to as normalized intensity) versus the NH_4^+ concentration in the calibration solutions.

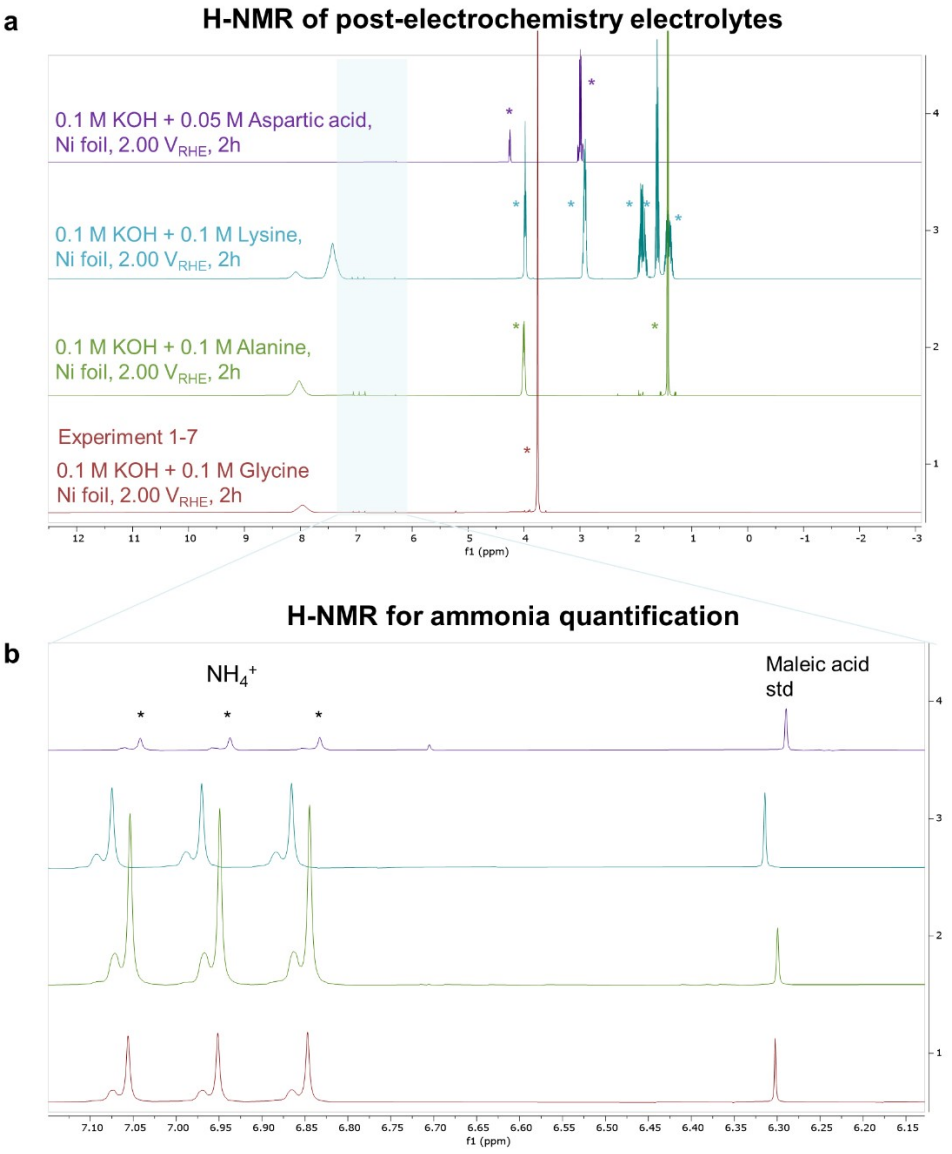

Figure S4. a) Representative H-NMR spectra of post-electrolysis electrolytes for the amino acids tested in this work. The H-NMR solution consists of 500 uL of post-electrolysis electrolyte, 50 uL of 4.0 M HCl, 25 uL of 3 mM Maleic acid and 63.8 uL of D_2O. H-NMR spectra were obtained on a 500.18 MHz Bruker AVANCE NEO spectrometer with water suppression. The asterisked (*) peaks denote the peaks of the corresponding amino acids. b) zoomed-in region showing the maleic acid standard, against which the triplet NH_4^+ peaks were quantified for faradaic efficiency calculation.

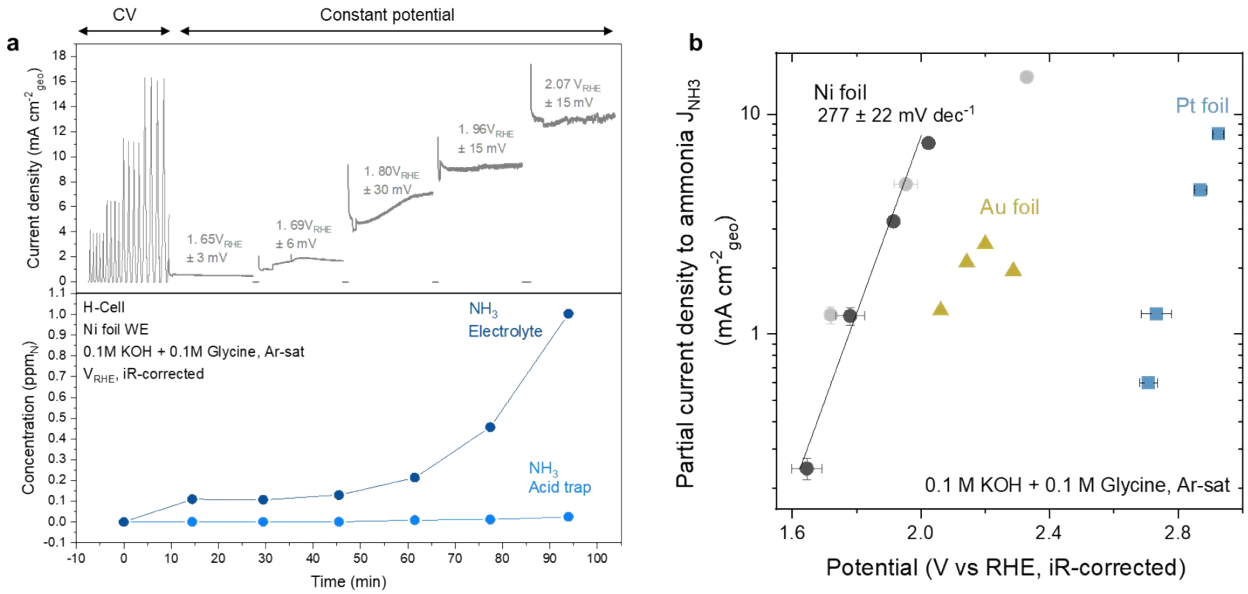

Figure S5. Screening of ammonia production from electrochemical glycine oxidation. a) Current density (top) and NH_3 concentrations (bottom) as a function of time. The electrochemistry began with cyclic voltammetry and then followed by constant potential holds for 15 mins with 1 min open circuit potential periods in between for analyte sampling. The iR-corrected potential is reported in grey labels above each of the chronoamperometry, where the uncertainty is derived from variation in the iR correction. Based on the figure, the ammonia generation begins at a highly oxidative potential >1.69 V_{RHE}. The NH_3 primarily resides in the electrolyte and not the acid trap. b) Tafel slope analysis between the partial current density to ammonia (J_{NH3}) and the RHE potential for Ni foil. Dark and light grey points indicate two separate screening experiments. A Tafel slope analysis in the linear region shows a slope of 277 ± 22 mV dec^{-1}. J_{NH3} is calculated by multiplying the NH_3 faradaic efficiency (obtained by calculating the produced ammonia during the chronoamperometry at each potential hold and using $z_e^- = 6$, see **Table 2** in the main text) with the average current density. The vertical and horizontal error bars were obtained from the standard deviation in the current density and the variation in the iR-correction, respectively. The uncertainty in the Tafel slope is obtained from the standard error of the fitted slope from linear regression of Potential vs $\log_{10}(J_{NH3})$. On the same plot, the ammonia partial current densities tested on Au foil (yellow) and Pt foil (blue), screened in the same way as Nickel (panel a), are also shown on the same plot, where ammonia production was found to be shifted to an even greater positive potential.

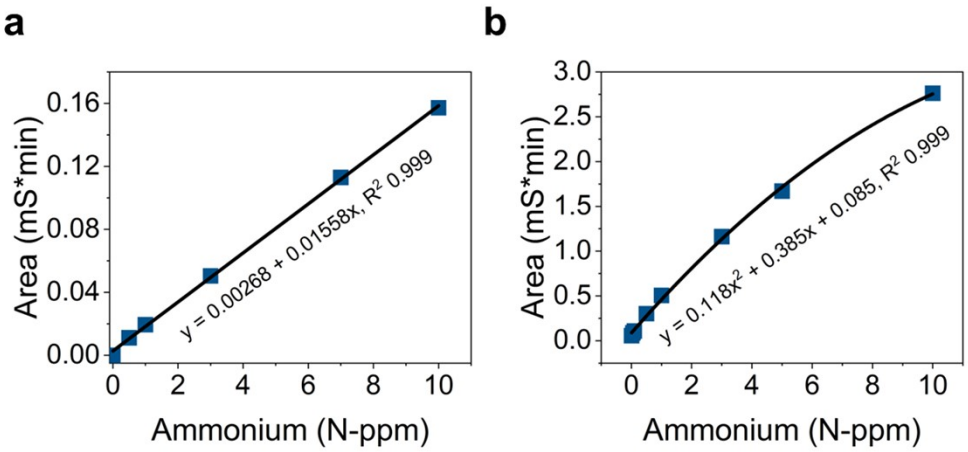

Figure S6. NH_4^+ calibration curve via Ion Chromatography done in 100mM of glycine with 100mM of KOH of a) institution 2 and b) institution 3. The dilution of the calibration curve is the same dilution factor by which the samples are diluted when measured.

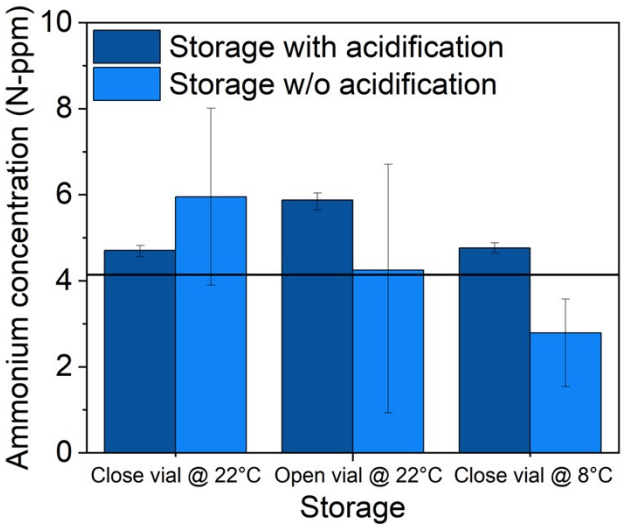

Figure S7. The influence of sample storage and acidification on quantification reliability of NH_4^+. NH_4^+ is quantified via ion chromatography after storage in a close vial, open vial, at 22°C and 8°C. Horizontal line marks the quantity measured the same day of the sample preparation. Sample acidification in a closed via appears to improve the reliability of NH_4^+ quantification.

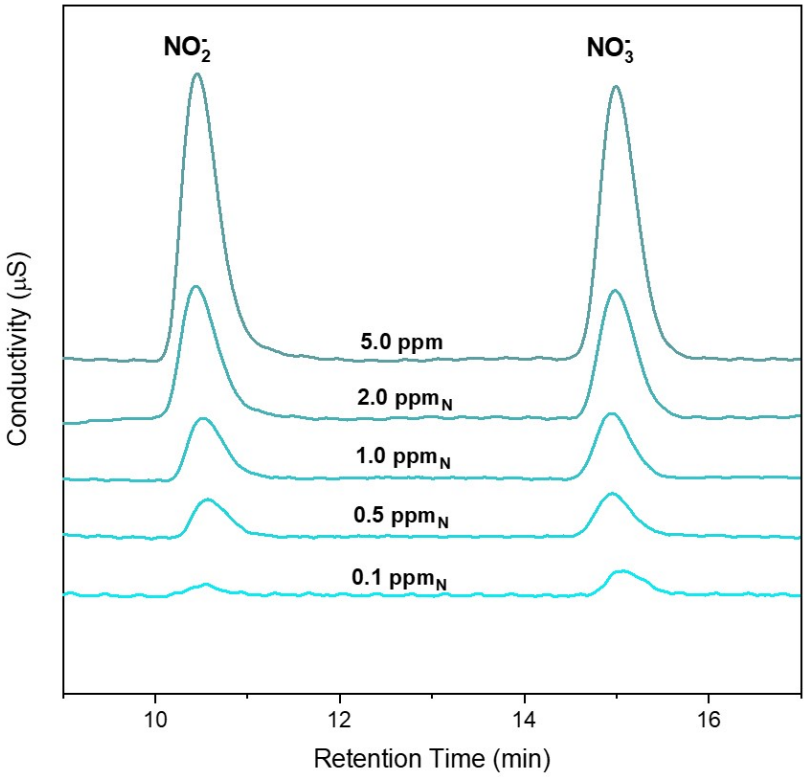

Figure S8. Representative Ion chromatogram of NO_2^- and NO_3^- calibration solutions prepared from appropriately weighed KNO_3 and KNO_2 dissolved in 0.1 M KOH and 0.1 M Glycine matrix. The chromatograms were measured by Institution 1.

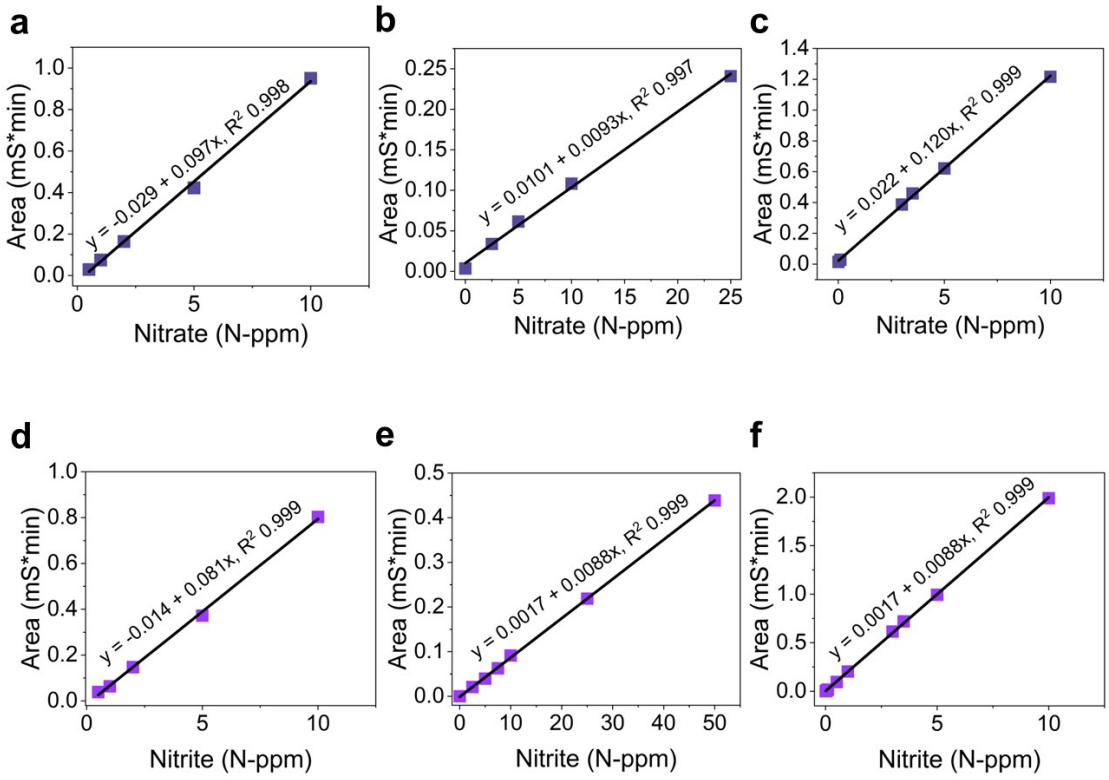

Figure S9. Calibration curves for NO_2^- and NO_3^- quantification. a), b), and c) NO_2^- and d), e), and f) NO_3^- calibration curve done in 0.1 M KOH and 0.1 M Glycine at institution 1, 2, and 3, respectively. The representative chromatogram can be found in **Figure S8**.

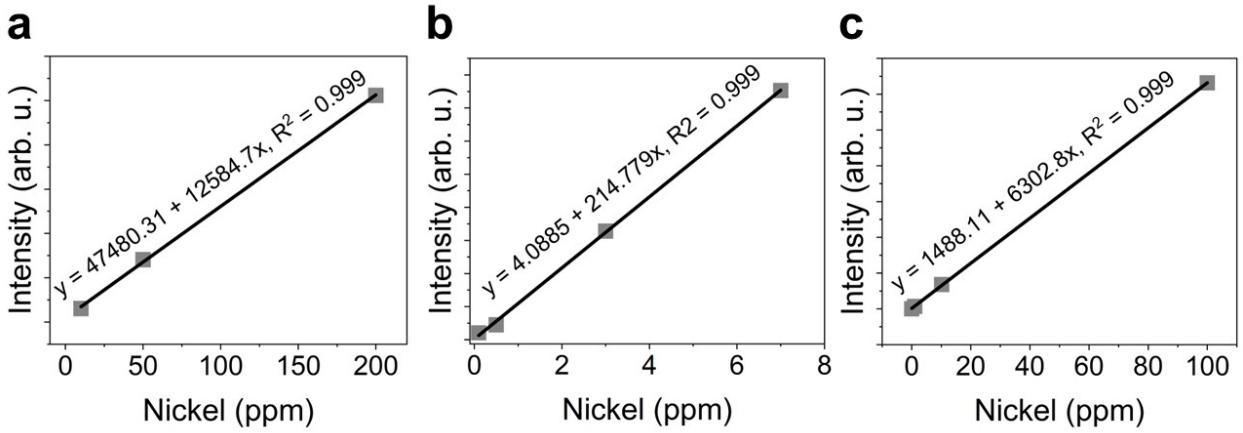

Figure S10. Representative ICP calibration curves of Ni^{2+} done in 2% nitric acid at a) institution 1 (ICP-MS), b) institution 2 (ICP-OES), and c) institution 3 (ICP-OES). The dilution of the calibration curve is the same dilution factor by which the samples are diluted. Calibration curves are generated at the beginning of each ICP session.

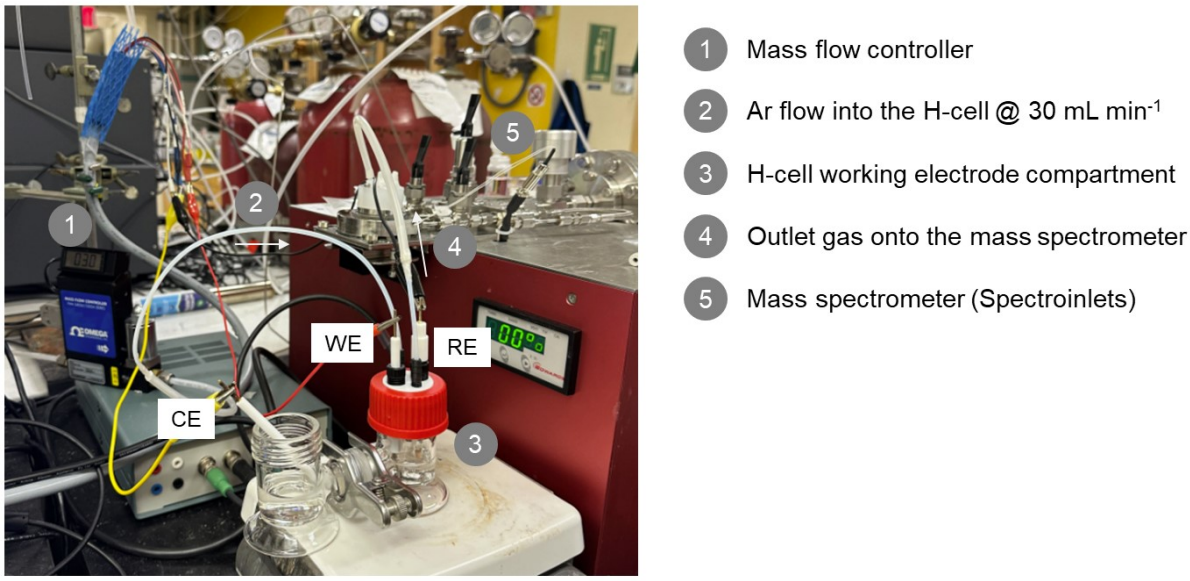

Figure S11. Experimental setup for gas detection during electrochemical amino acid oxidation established at Institution 1. A mass flow controller configured at 30 mL min^{-1} controls Ar flow into the H-cell. The outlet is connected to the aqueous cell which sits on top of the on-chip electrochemistry mass spectrometer (EC-MS). In a typical measurement, the H-cell consists of a 0.5 x 1 cm^2_{geo} polished Ni foil, Ag/AgCl (3.0 M KCl) and Pt mesh as the working, reference and counter electrodes respectively, as well as an anion exchange membrane separating 20 mL of electrolytes from each compartment.

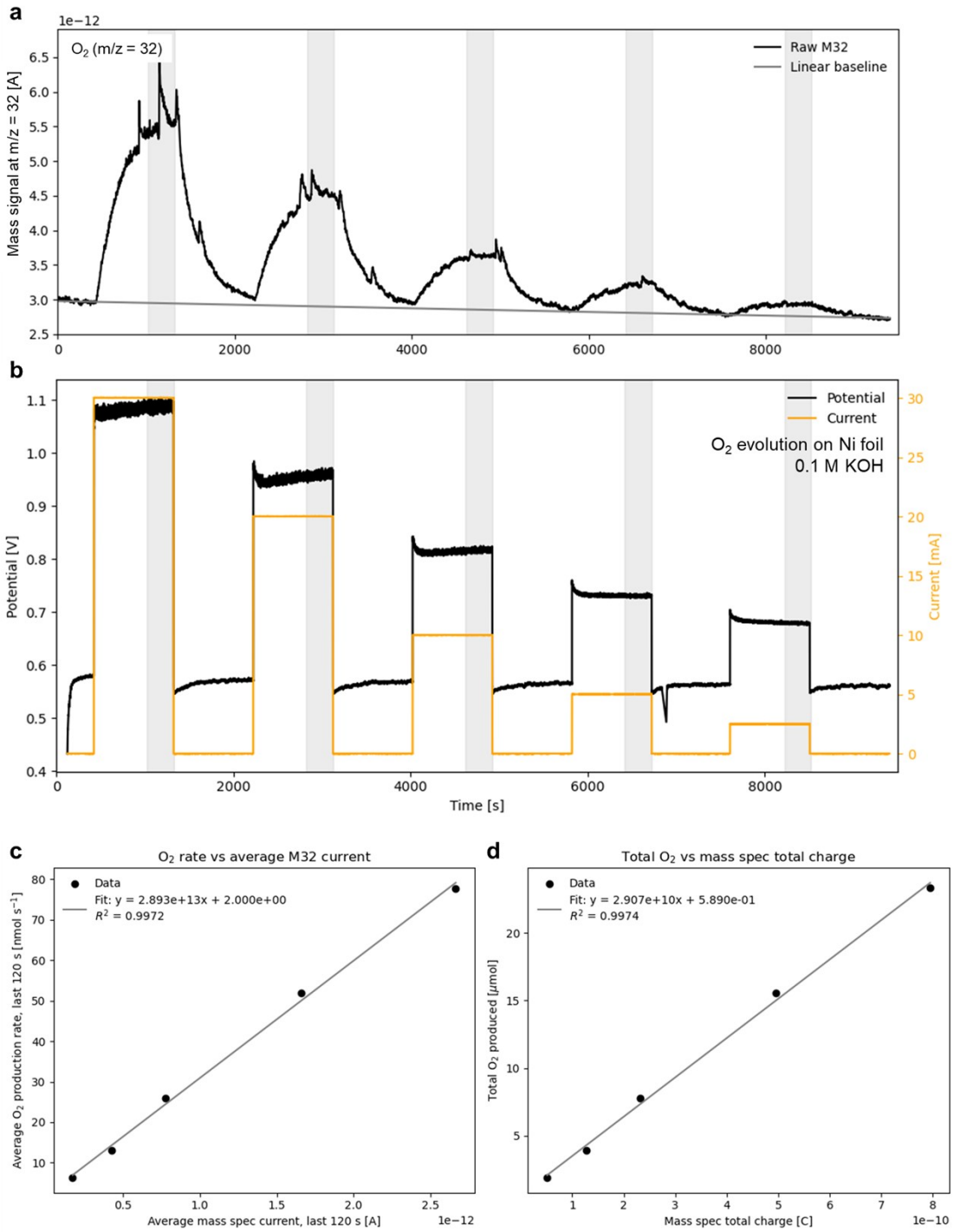

Figure S12. Calibration of O_2 for quantification and calculation of faradaic efficiency. Mass spectrometer signal at m/z = 32 (b) and the associated electrochemical program (b) are shown, consisting of 10 min constant current holds at 30 mA, 20 mA, 10 mA, 5 mA and 2.5 mA (yellow) with Ni foil in 0.1 M KOH, followed by 15 min open circuit potential periods in between. During this calibration measurement, the H-cell was connected to the mass spectrometry in the manner shown in **Figure S11**. The H-cell consists of a 0.5 x 1 cm^2_{geo} polished Ni foil, Ag/AgCl (3.0 M

KCl) and Pt mesh as the working, reference and counter electrodes respectively, as well as an anion exchange membrane separating 20 mL of electrolytes from each compartment. In the O_2 mass signal (panel a), a linear baseline is drawn to account for the signal drift of the mass spectrometer. Panels (c) and (d) show the O_2 calibration curves with respect to the O_2 production rate and O2 produced respectively. The O_2 production rate and O_2 mol produced were calculated from the applied current (in mA) by assuming 100% faradaic efficiency to O_2 evolution with n_{e^-} = 4 (see **Table 2**). The corresponding mass spectrometer signal and mass spectrometer current were obtained by averaging last 2 mins of the signal from each of the 15 min constant current holds as shown in the shaded region in panels a-b, over which the mass spectrometer m/z = 32 signal has stabilized.

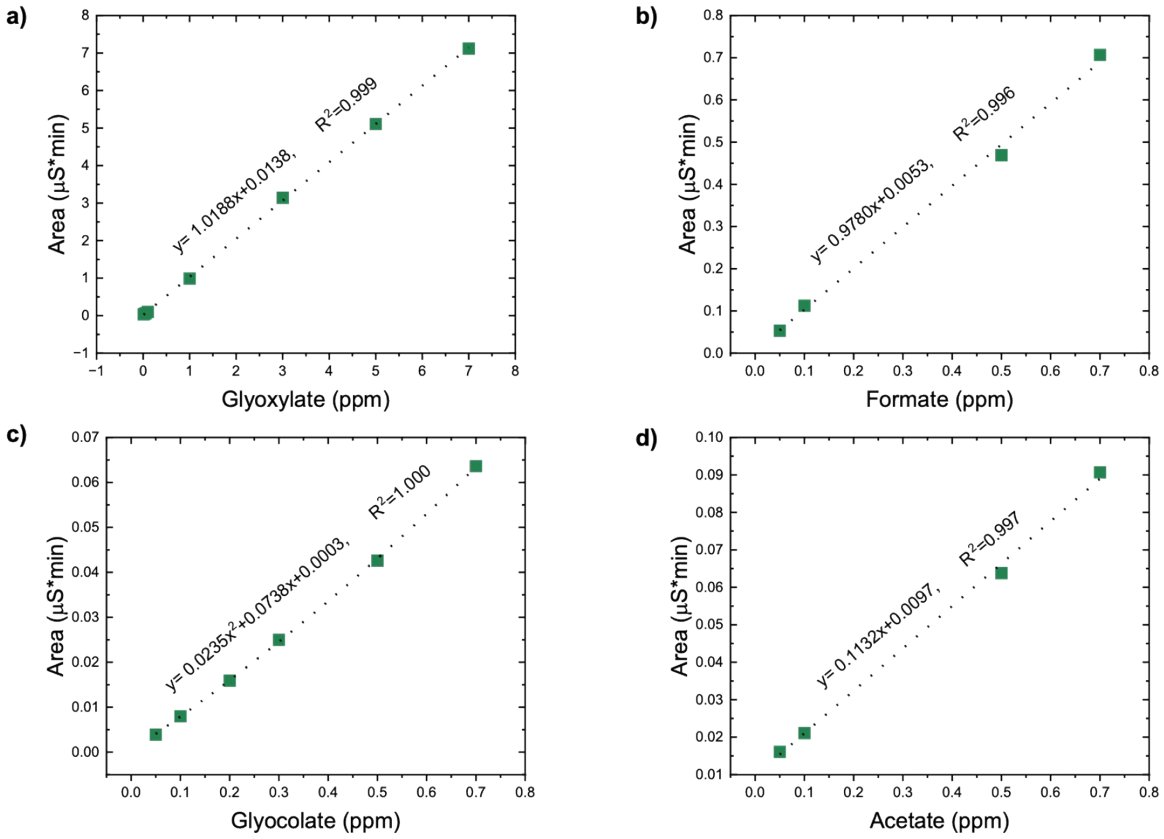

Figure S13. IC calibration curves of glyoxylate (a), formate (b), glycolate (c) and acetate (d) done in 0.1 M glycine and 0.1 M KOH. The dilution of the calibration curve is the same dilution factor by which the samples are diluted.

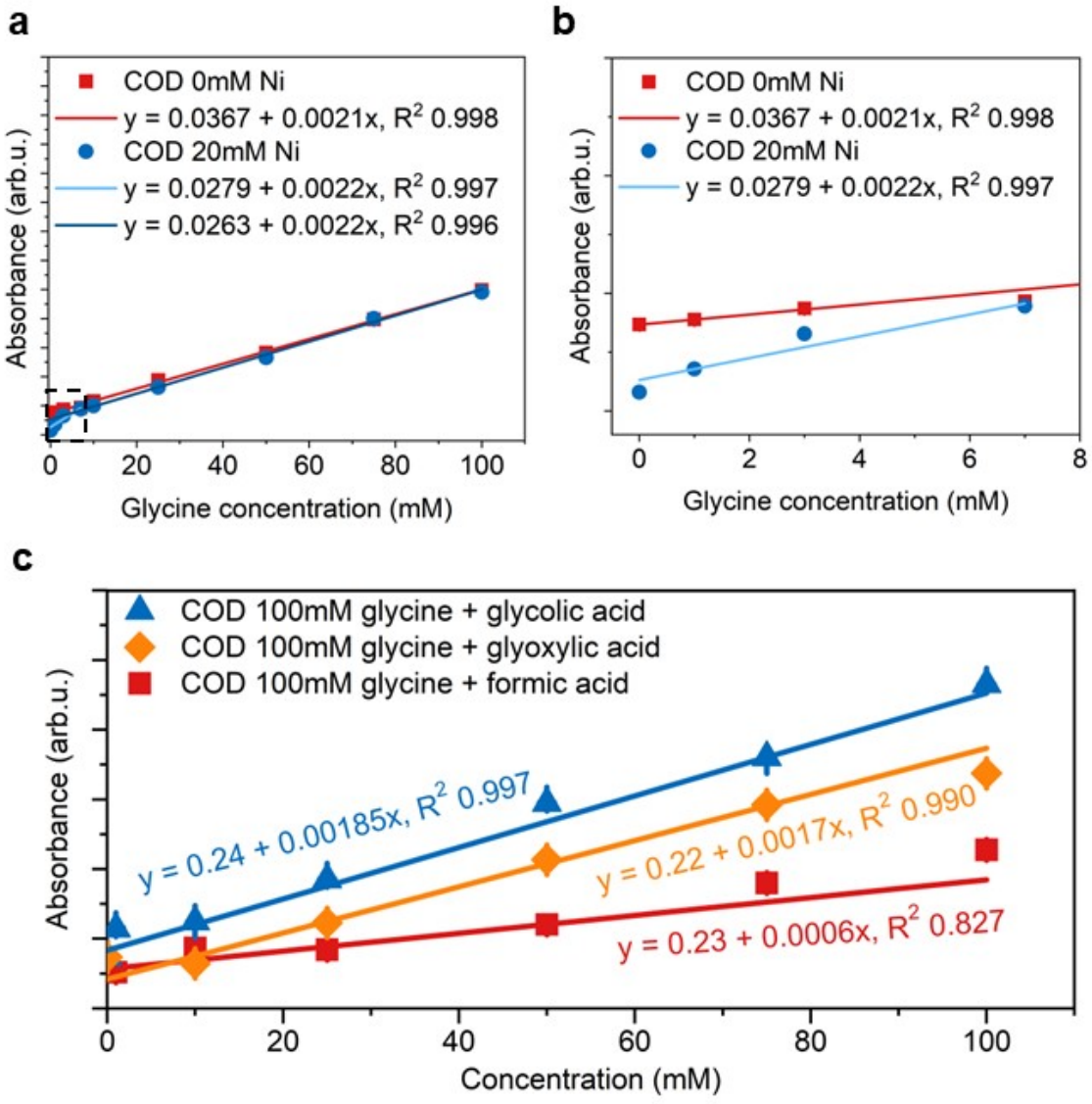

Figure S14. Chemical oxygen demand measurements for glycine detection in 100mM of KOH with 0 mM and 20 mM of Ni^{2+} ions present in solution. a) shows 0 mM to 100mM of glycine, b) shows a zoom in of the region of 0 mM to 8 mM, marked as dash lines in a). c) Chemical oxygen demand measurements of 100 mM KOH and 100 mM glycine with different concentrations of glycolic acid, glyoxylic acid, and formic acid.

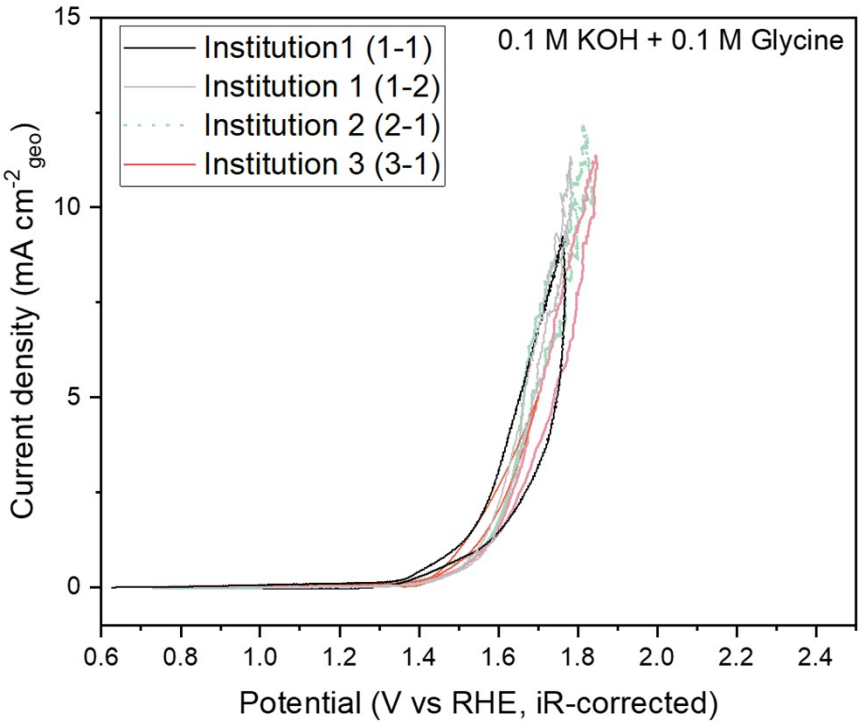

Figure S15. Comparison of cyclic voltammetry curves of Ni foil in 0.1 M KOH + 0.1 M Glycine. In accordance with the benchmarking protocol, the Ni foil was previously electrochemically polished in H_3PO_4 and OER cycled in 0.1 M KOH prior to the glycine experiment. Representative curves for comparison showed good agreement across institutions.

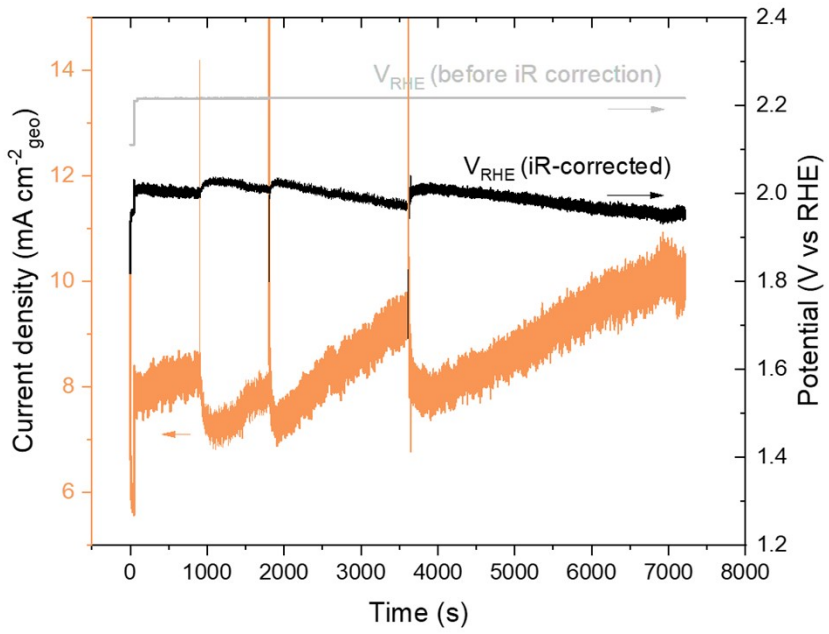

Figure S16. Demonstration of potential conversion to the RHE scale during chronoamperometry. Current density (orange, left axis), Potential vs RHE before (grey, right axis) and after iR-correction (black, right axis) during the 2 hour electrolysis are shown. The Potential vs RHE before iR correction is obtained following equation 1 (see **Supplementary Note 2**), using +0.197 V vs SHE for Ag/AgCl (sat. KCl) reference electrode and solution pH of 10.7 for 0.1 M KOH + 0.1 M Glycine. The IR-corrected potential is computed by subtracting it with the term *i(t)*R*, where i(t) is the current density at time t (orange curve) and R is the solution resistance measured via the zero real Z intercept at high frequency from impedance spectroscopy.

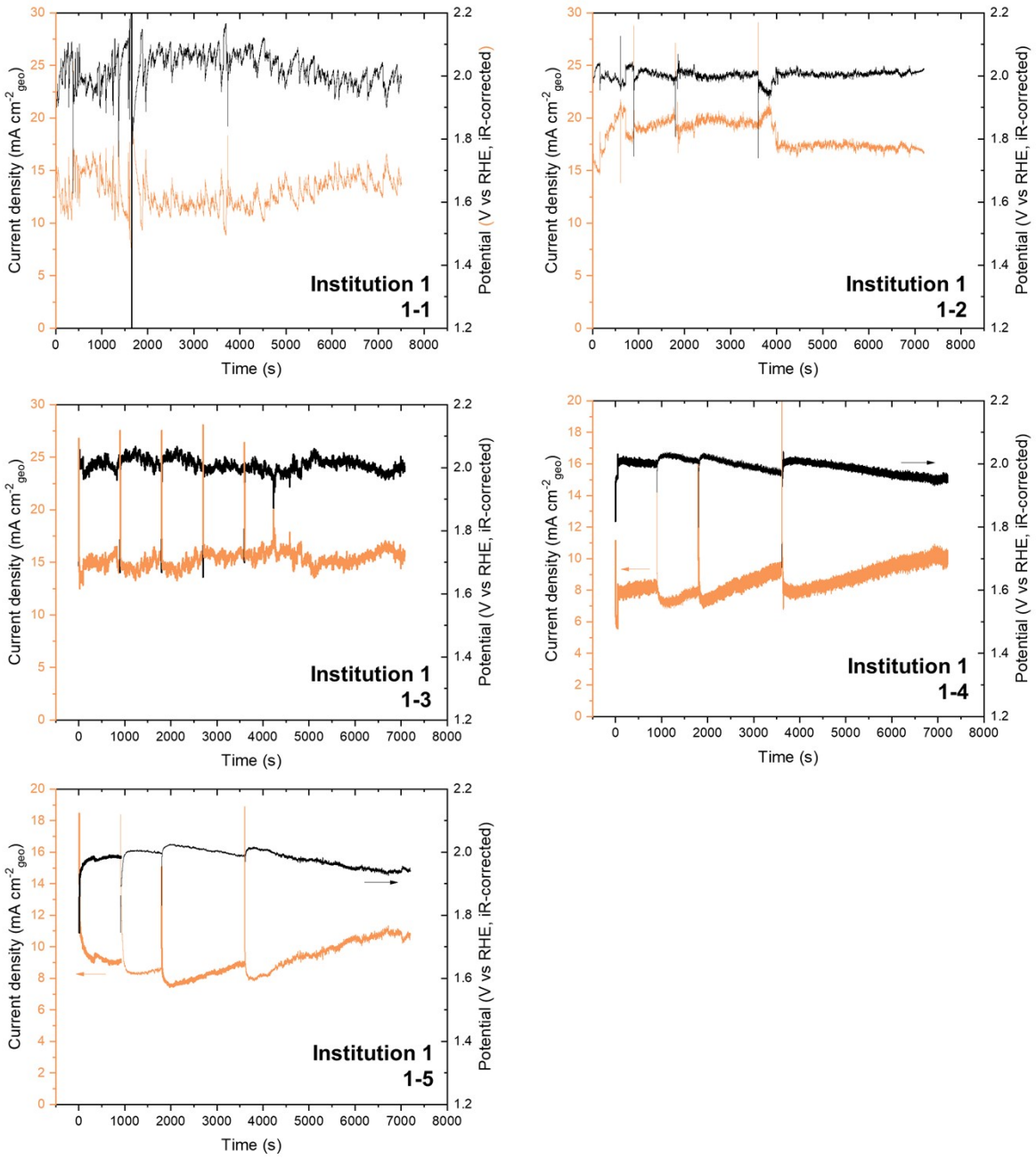

Figure S17. Chronoamperometry profiles of electrochemical glycine oxidation on Ni foil electrode at 2.00 V_{RHE} over 2 hours (i.e. 'benchmarking') across trials by Institution 1. The averaged and standard deviation in the iR-corrected potentials are tabulated in **Table S1**.

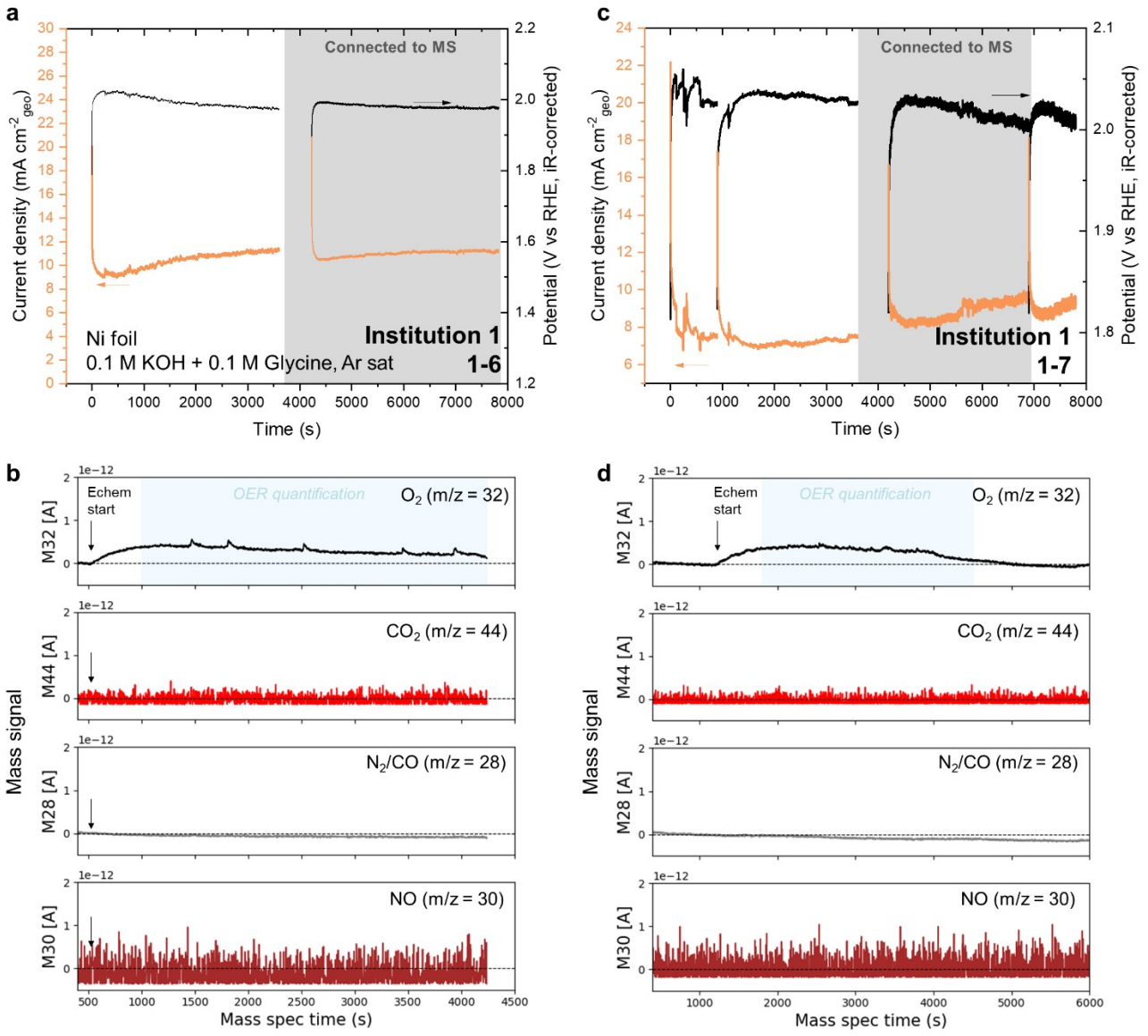

Figure S18. Chronoamperometry profiles of experiments 1-6 (a-b) and 1-7 (c-d) during electrochemical glycine oxidation on Ni foil electrode at 2.00 V_{RHE} over 2 hours (i.e. 'benchmarking'). The region shaded in grey corresponds to the period when the H-cell was connected to the mass spectrometer in the manner described in **Figure S11**. Panels (b) and (d) are the corresponding mass spectrometer signal at m/z = 32, 44, 28 and 30, where the spectra have been background-subtracted by the baseline signal, defined as the average of the signal before the start of electrochemical program over a period 120 s. Only O_2 (m/z = 32) was observed during glycine oxidation. To obtain O_2 faradaic efficiency, O_2 was quantified by averaging the mass spectrometer signal over the period shaded in blue i.e. when the mass spectrometer signal has stabilized) and converting it to O_2 production rate using the calibration curve established in Panel c of **Figure S12**.

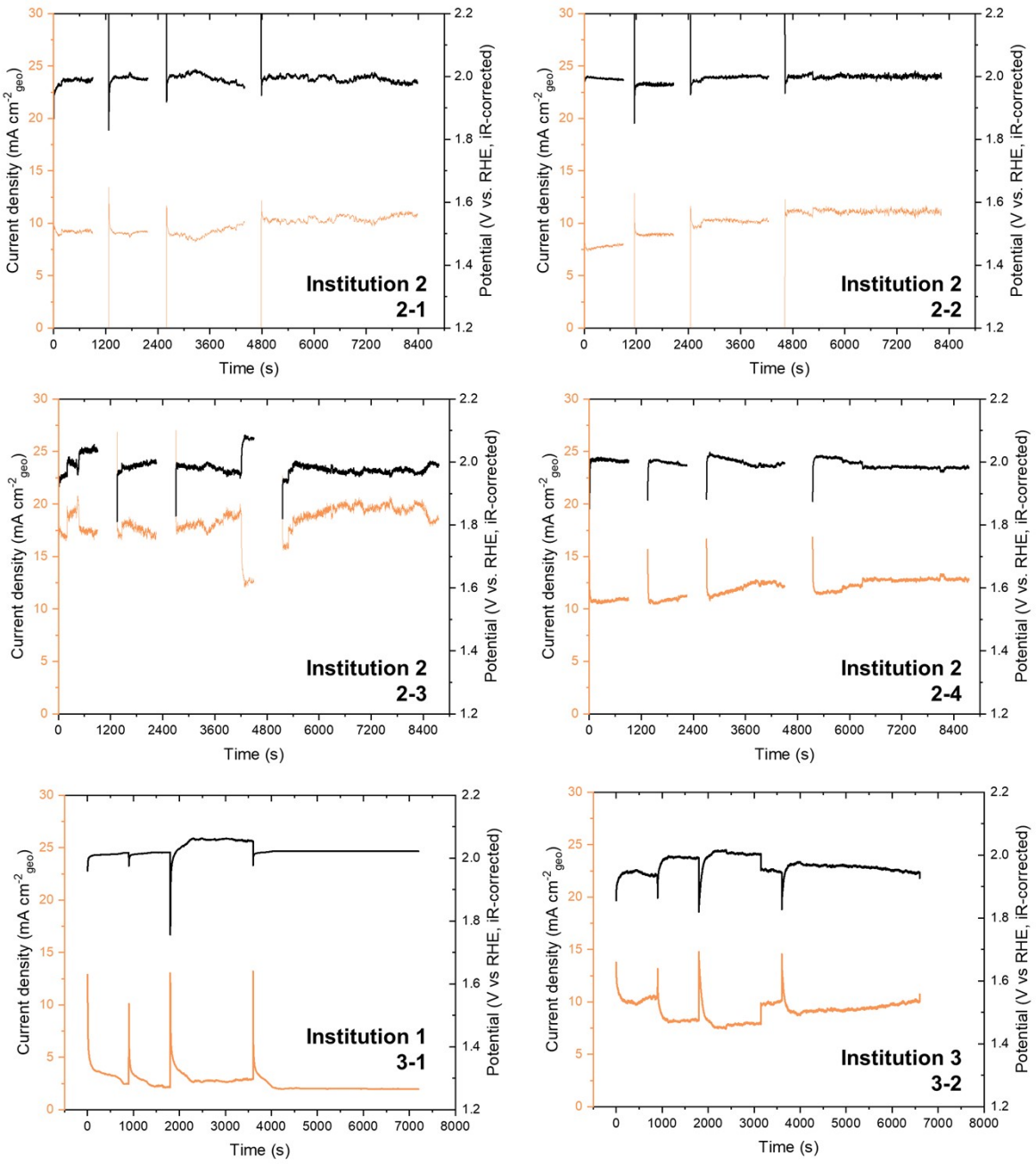

Figure S19. Chronoamperometry profiles of electrochemical glycine oxidation on Ni foil electrode at 2.00 V_{RHE} over 2 hours across trials by Institution 2 and Institution 3. The averaged and standard deviation in the iR-corrected potentials are tabulated in **Table S1**.

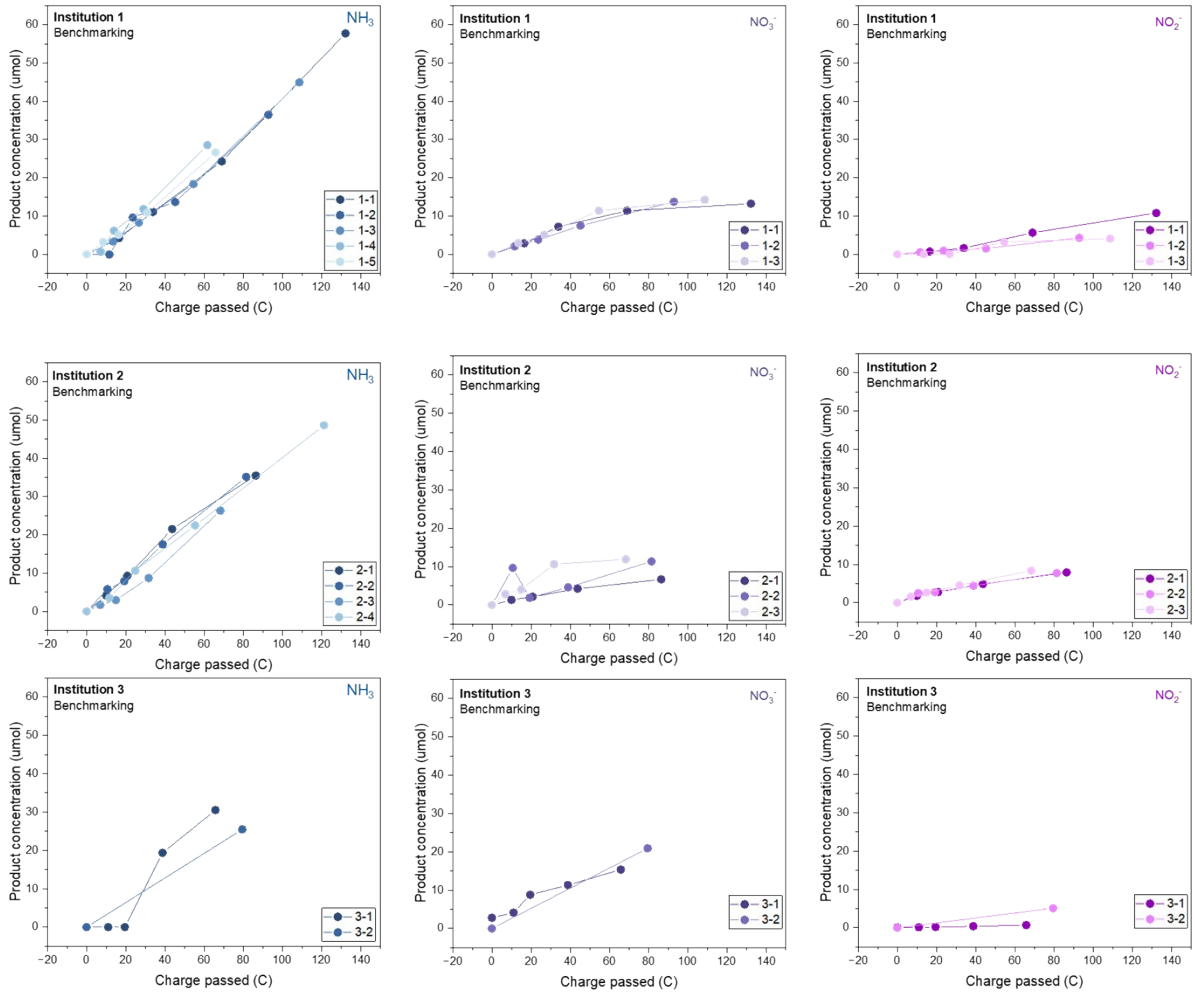

Figure S20. Concentrations of NH_3 (blue), NO_3^- (purple) and NO_2^- (magenta) as a function of passed charge during electrochemical glycine oxidation on Ni foil electrode at 2.00 V_{RHE} over 2 hours (i.e. 'benchmarking' condition). Data of multiple repeats by Institution 1, 2 and 3 are shown in the top, middle and bottom rows respectively.

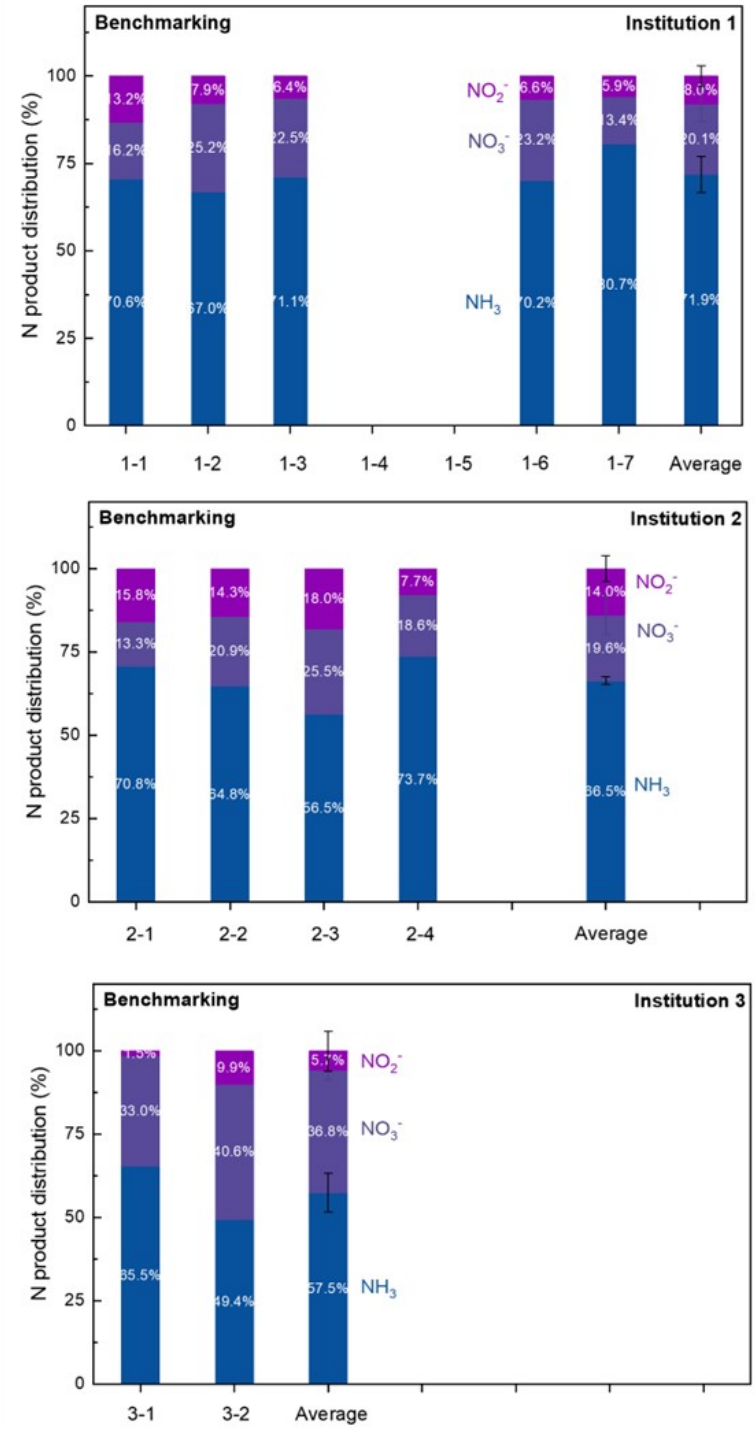

Figure S21. Nitrogen product distribution across NH_3 (blue), NO_3^- (purple) and NO_2^- (magenta) across repeats by institution 1 (top row), institution 2 (middle) and institution 3 (bottom) during electrochemical glycine oxidation on Ni foil electrode at 2.00 V_{RHE} over 2 hours (i.e. 'benchmarking' condition). N product distribution is calculated by calculating the mol fraction each product from the sum of NH_3, NO_3^- and NO_2^-.

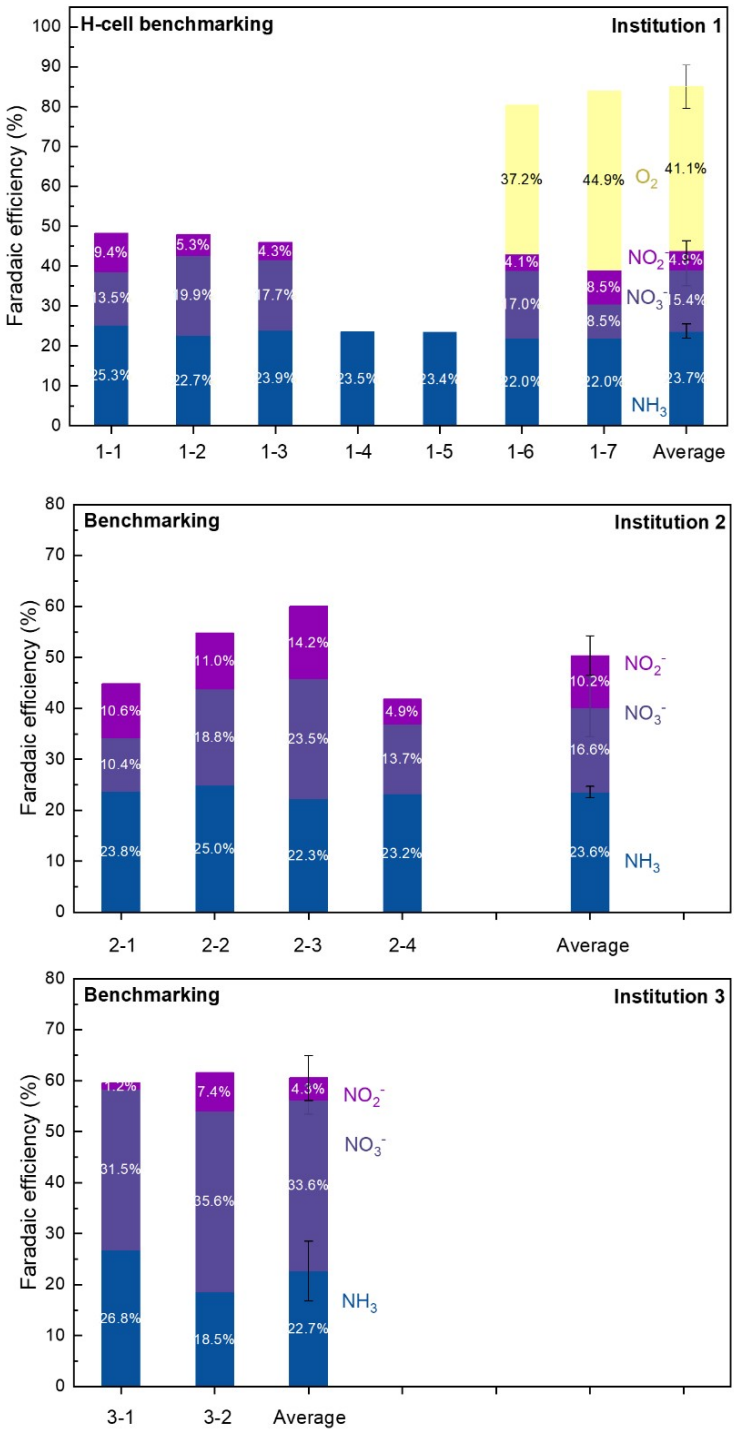

Figure S22. Faradaic efficiency of NH_3 (blue), NO_3^- (purple) and NO_2^- (magenta) across repeats by institution 1 (top row), institution 2 (middle) and institution 3 (bottom) during electrochemical glycine oxidation on Ni foil electrode at 2.00 V_{RHE} over 2 hours (i.e. 'benchmarking' condition). The Faradaic efficiency is calculated with ne- = 6, 14,12 and 4 for NH_3, NO_3^-,NO_2^- and O_2 respectively (see Table 2 in Experimental section of the main text for the half-cell equations and assumptions).

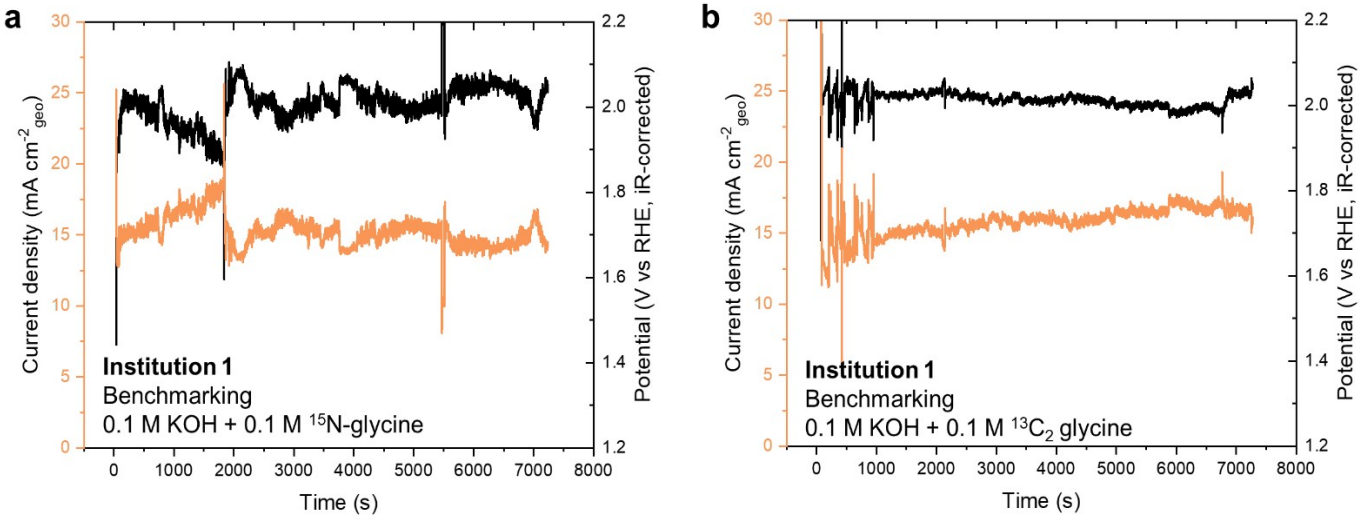

Figure S23. Chronoamperometry profiles of the isotope labelling experiments with ^{15}N-glycine (a) and $^{13}C_2$-glycine (b) during electrochemical glycine oxidation on Ni foil electrode at 2.00 V_{RHE} over 2 hours (i.e. 'benchmarking' condition). It is noted that the ^{15}N-glycine experiment suffered from greater current fluctuations leading to larger variations in the applied potential around the intended 2.00 V_{RHE} after iR-correction.

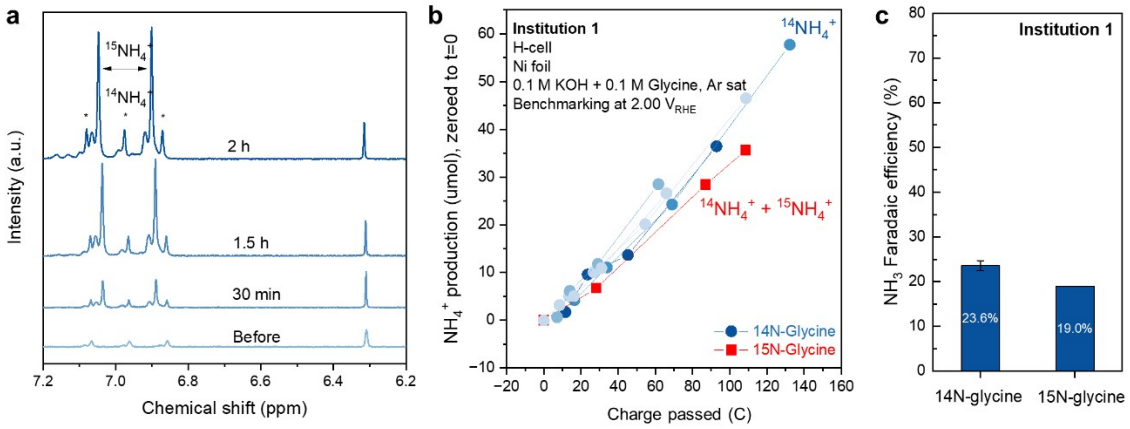

Figure S24. Product analysis from benchmarking experiment (electrochemical glycine oxidation on Ni foil electrode at 2.00 V_{RHE} over 2 hours) with 0.1 M KOH and N-labelled glycine. a) H-NMR spectra of the analytes before electrolysis and after 30 min, 1.5 h and 2 h electrolysis. A doublet $^{15}NH_4^+$ peak prominently grew with longer electrolysis time. However, a non-negligible $^{14}NH_4^+$ in the before electrolysis sample (i.e. ~3 ppm_N in the as-made 0.1 M KOH + 0.1 M ^{15}N-glycine) and the growth of the triplet $^{14}NH_4^+$ peaks over time indicates the production of non-labelled ammonia, which we attribute partly to the isotopic impurity of the commercial ^{15}N-glycine. b) Ammonia production from the ^{15}N-glycine experiment (red) compared to the non-labelled glycine (blue) as a function of charge passed. c) NH_3 faradaic efficiency of the ^{15}N-glycine experiment under the 'benchmarking' condition was found to be 19%, which is rather lower than the non-labelled glycine. We attribute this difference to the less stable chronoamperometry when ^{15}N-glycine is used (**Figure S23a**), which led to less precise control of the applied potential around the 2.00 V_{RHE} after iR-correction.

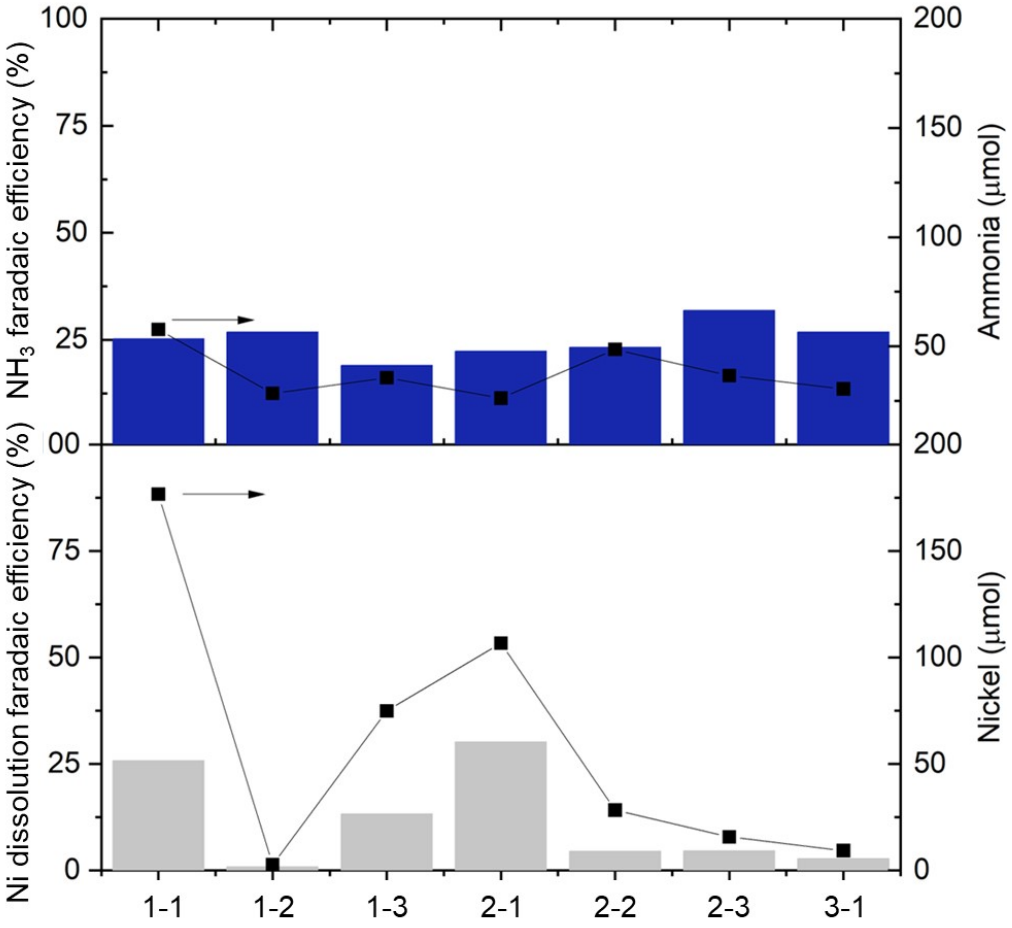

Figure S25. Ammonia and nickel measurements of all three institutions (where 1-1 denotes Institution 1, experiment 1) showing the inconsistency in nickel leaching into solution despite the consistent level of ammonia production. Left Y axis shows the faradaic efficiencies of ammonia (top) and nickel (bottom), and right Y axis is the quantification of ammonia (top) and nickel (bottom) in µmol. Ammonia production is consistent cross-institutionally across multiple repeats, but the Ni dissolution showed significant discrepancies.

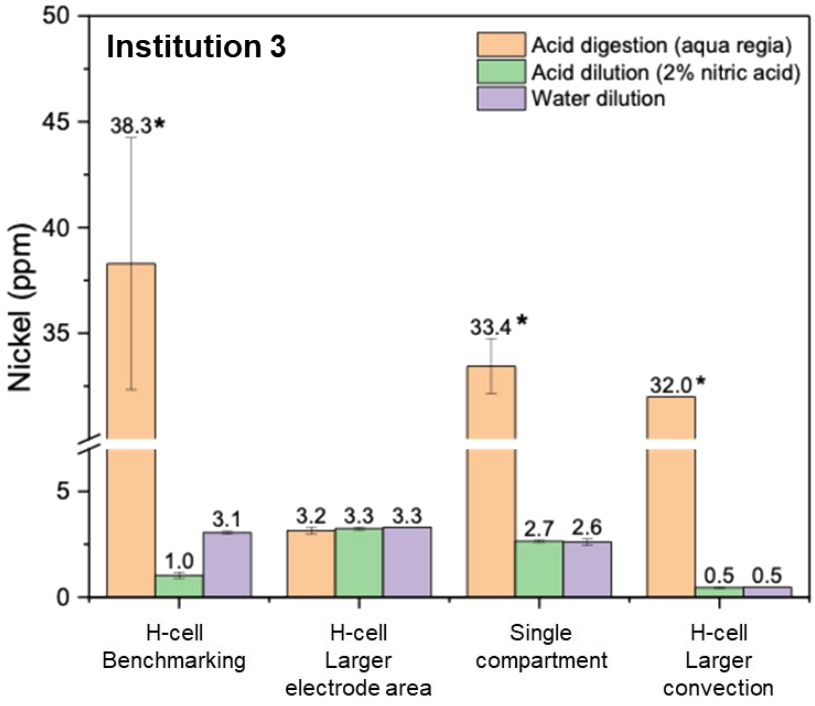

Figure S26. Nickel dissolution behavior quantified as dissolved Ni concentration (ppm) during electrolysis in 0.1 M glycine + 0.1 M KOH under multiple reactor configurations, including the benchmarking condition, increased electrode area, undivided cell operation, and enhanced convection. * denotes samples analyzed approximately five months earlier following aqua-regia acid digestion, whereas non-asterisked samples were prepared and measured at the same time. Apart from the benchmarking condition, all configurations exhibited strong agreement between acid-diluted and water-diluted sample preparation methods. Acid-digested samples consistently yielded higher apparent Ni concentrations in the older samples. However, for the increased electrode area configuration, acid digestion produced comparable Ni concentrations to other methods when analyzed on the same day, indicating good reproducibility of sample preparation methods; observed discrepancies are attributed primarily to long-term sample storage prior to analysis.

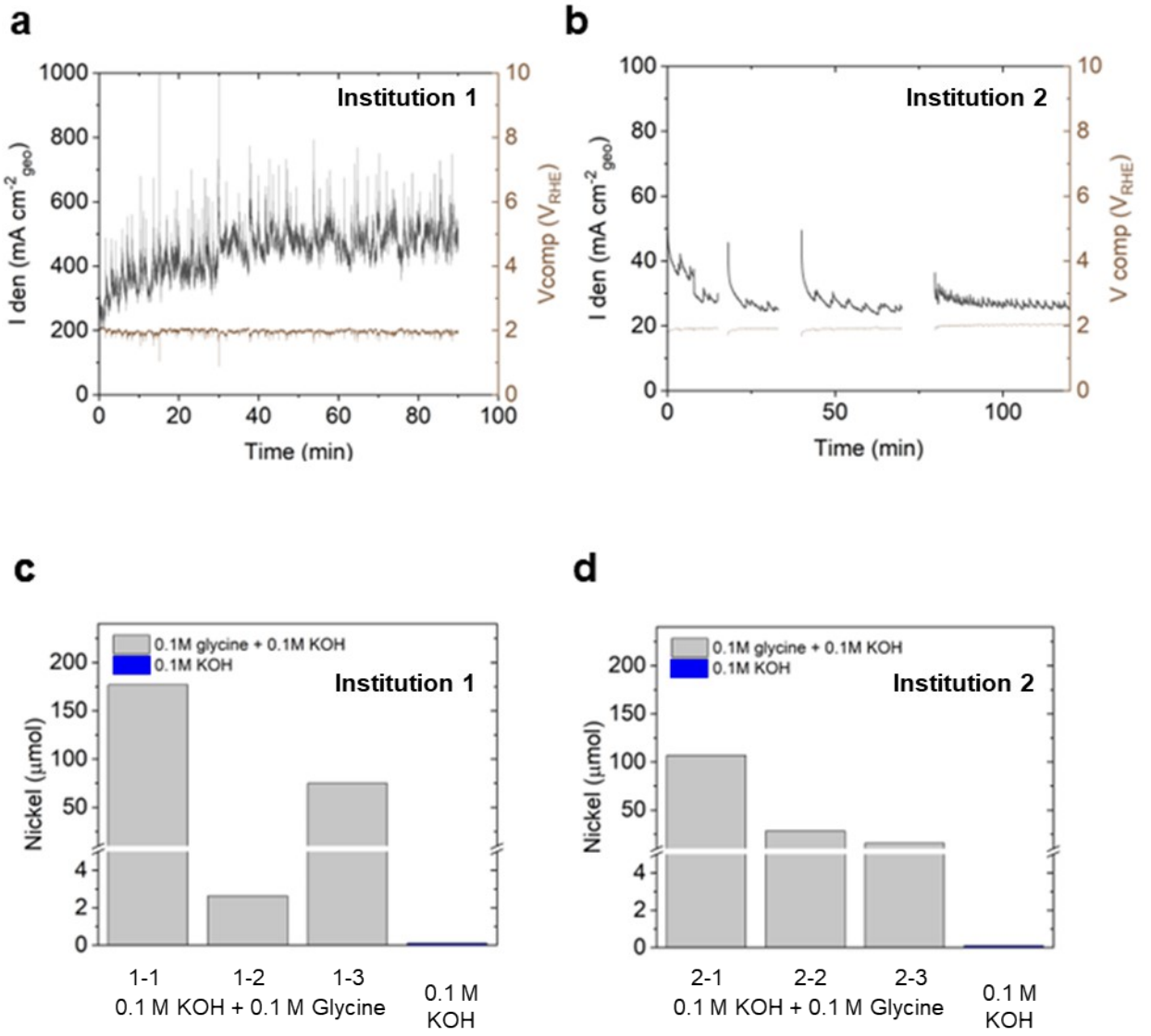

Figure S27. Oxygen evolution reaction (OER) electrolysis data on Ni foil (0.1 M KOH) a) institution 1 and b) institution 2. For institution 1, the electrode area employed is 0.1 x 0.15 cm^2 (0.03 cm^{-2}_{geo}). The smaller electrode was employed to avoid potentiostat overload. Comparison of Ni corrosion (µmol) during OER (0.1 M KOH) and glycine oxidation (0.1 M glycine in 0.1 M KOH) by c) institution 1 and d) institution 2. The Ni^{2+} dissolution in the glycine-absent electrolyte (0.1 M KOH) was measured to be <0.1 umol over the 2 hour electrolysis, suggesting the significantly enhanced instability of Ni in the presence of glycine or other analogously liganding amino acids.

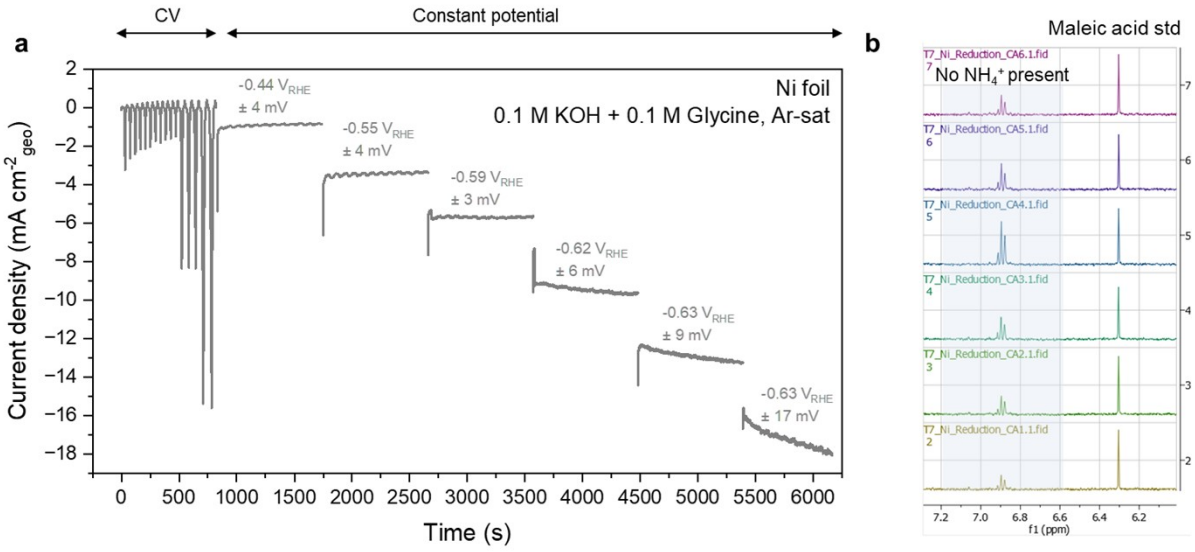

Figure S28. a) Screening of electrochemical reduction of 0.1 M KOH + 0.1 M Glycine on Ni foil. The electrochemistry began with cyclic voltammetry and then followed by constant potential holds for 15 mins with short open circuit potential periods in between for analyte sampling. The iR-corrected potential is reported in grey labels above each of the chronoamperometry (CA), where the uncertainty is derived from variation in the iR correction. b) H-NMR spectra of the electrolyte sampled after each CA hold. No characteristic NH_4^+ triplet peak was found, suggesting that ammonia liberation does not occur upon electrochemical reduction.

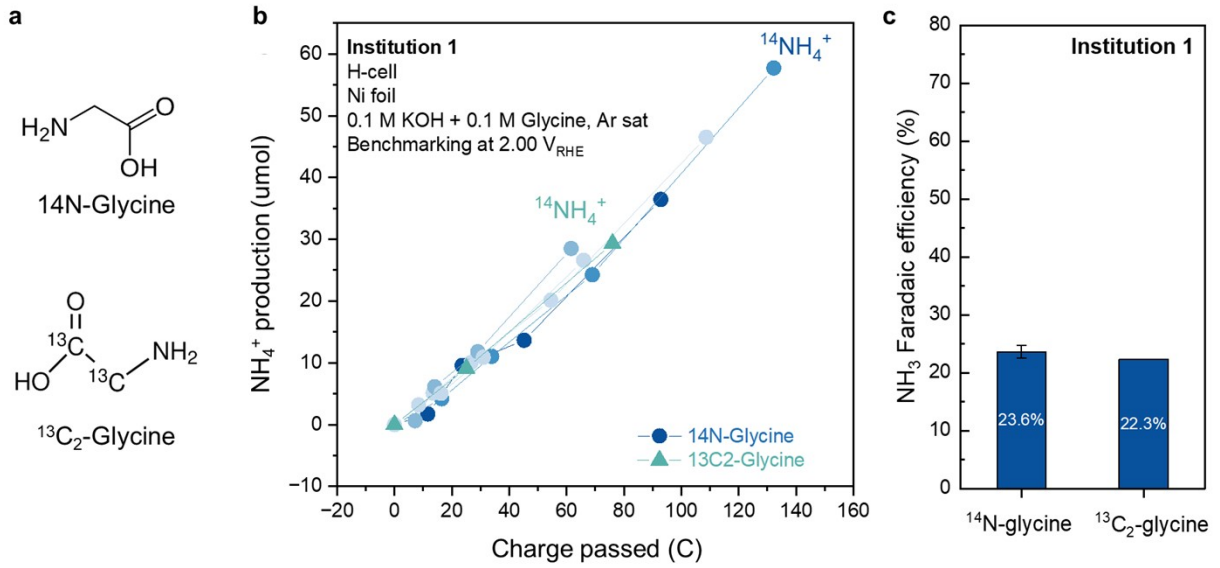

Figure S29. a) Schematic of unlabeled glycine (^{14}N-Glycine) and carbon-labelled glycine (13C2-Glycine), where both carbons are labelled. b) Ammonia production from the 13C2-glycine experiment (green) compared to the non-labelled glycine (blue) as a function of charge passed. The corresponding electrochemistry for the $^{13}C_2$-glycine experiment can be found in **Figure S23**. c) NH_3 faradaic efficiency of the $^{13}C_2$-glycine experiment under the 'benchmarking' condition was found to be 22.3%, which is in excellent agreement with the unlabeled glycine experiment by Institution 1.

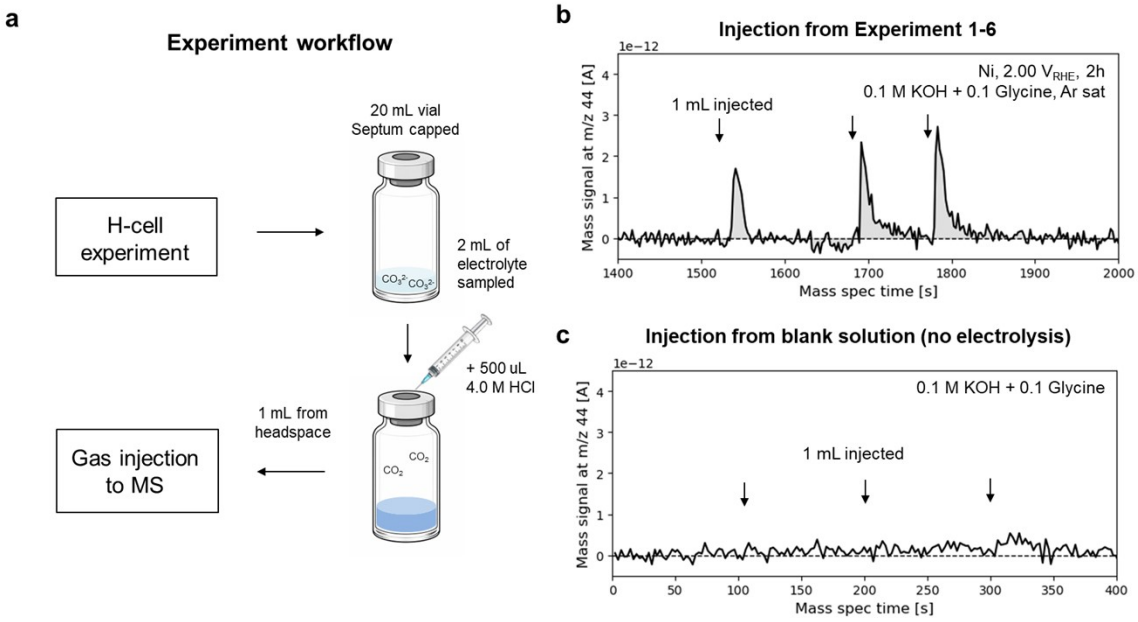

Figure S30. a) Experimental workflow for CO_3^{2-} quantification via electrolyte acidification. A 2 mL aliquot of post-electrolysis electrolyte was treated with 500 µL of 4.0 M HCl, releasing CO_2 into the headspace of an air-tight, septum-capped vial. b) Injection of 1000 µL of the headspace from a vial containing electrolyte after 2 h of electrochemical glycine oxidation ('benchmarking' condition), showing distinct CO_2 signals at m/z = 44. c) Injection of 1 mL of the headspace from a vial containing acidified stock electrolyte (0.1 M KOH + 0.1 M glycine), showing no detectable CO_2. This control confirms that CO_3^{2-} formation during electrolysis is well above the background CO_2 level arising from ambient air exposure.

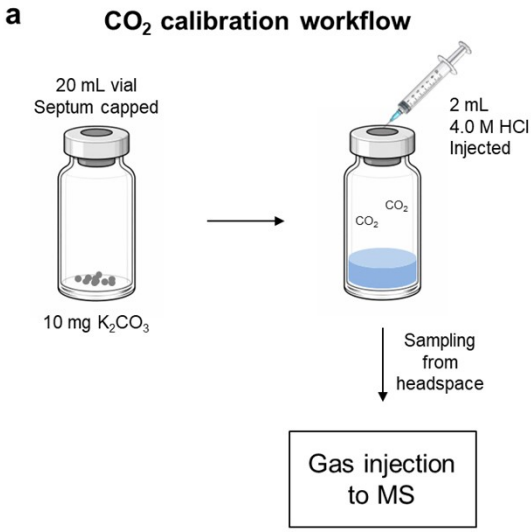

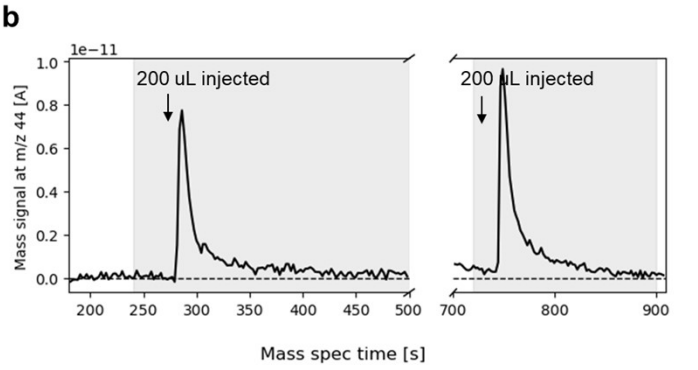

c

Injection	Volume sampled from headspace (uL)	CO_2 mol (umol)	Mass signal integration (C)	Calibration factor ($umol_{CO2}$/C)
1	200	0.72	1.82E-10	3.99E+09
2	200	0.72	2.14E-10	3.38E+09
3	400	1.45	3.78E-10	3.82E+09
			Average	3.73E+09

Figure S31. a) Experimental workflow for CO_2 calibration. A known quantity of potassium carbonate (K_2CO_3, Sigma, ACS Reagent, ≥99.0) was acidified with excess 4.0 M HCl in an air-tight septum-capped vial. The vial was then incubated for 10 mins prior to headspace sampling. The mol of CO_2 in the 20 mL vial was then determined assuming full 1:1 conversion from K_2CO_3 to CO_2 and negligible gas solubility in the acidic solution. b) Representative m/z=44 mass spectrometry signal from the CO_2 injections. The spectrum has been background subtracted by the baseline signal, defined as the average over 120 s prior to measurement. The shaded region indicates the area over which the mass signal is integrated for quantification c) Calculation of the calibration factor (i.e. the ratio of CO_2 quantity to the mass spectrometry signal, in $umol_{CO2}$ and Coulomb (C) respectively.

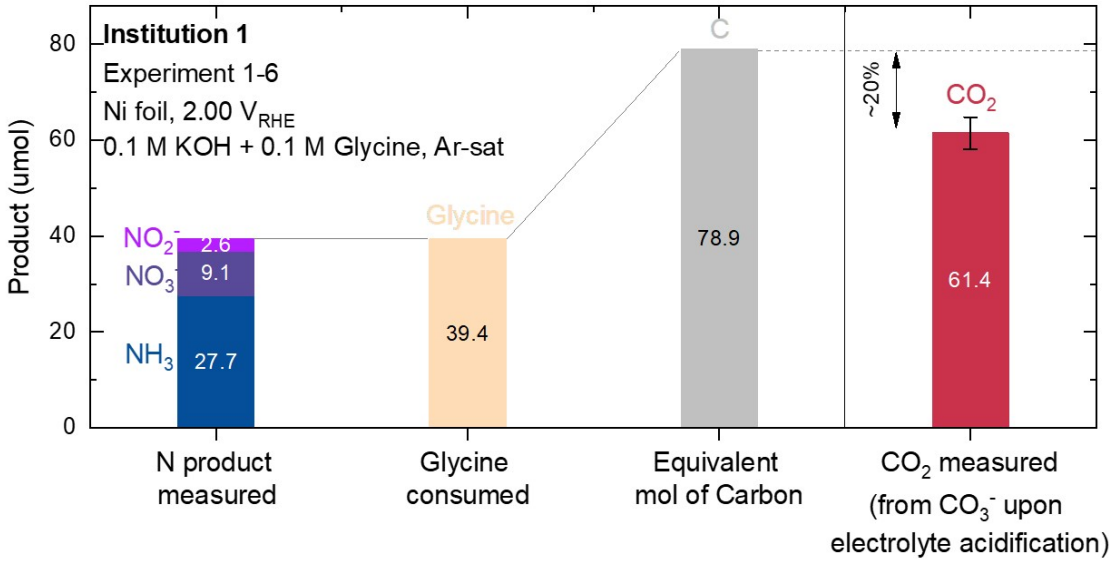

Figure S32. Carbon balance accounting from electrochemical glycine oxidation on Ni foil at 2.00 V_{RHE} from experiment 1-6 (see **Figures S18** and **Table S1**). The first bar showed the sum of nitrogen products (NH_3, NO_3^- and NO_2^-) experimentally quantified via H-NMR and ion chromatography. The second bar shows the equivalent glycine consumed during electrolysis, calculated based on the conservation of N atoms since each glycine molecule (NH_2CH_2COOH) possesses one N atom. The third bar shows the equivalent mol of carbon based on the conservation of C atoms, as each glycine molecule constitutes two C atoms. The final bar represents CO_2 quantified via post-electrolysis electrolyte acidification (see **Figure S31**), corresponding to ~80% of the carbon equivalents of consumed glycine. The remaining unclosed carbon balance (~20%) likely corresponds to the other carbon products detected in this work, such as formate, glycolate and glyoxylate which are not quantified in this experiment but characterized more broadly in this work (see **Figure 3** and **Figure 5** of the main figure).

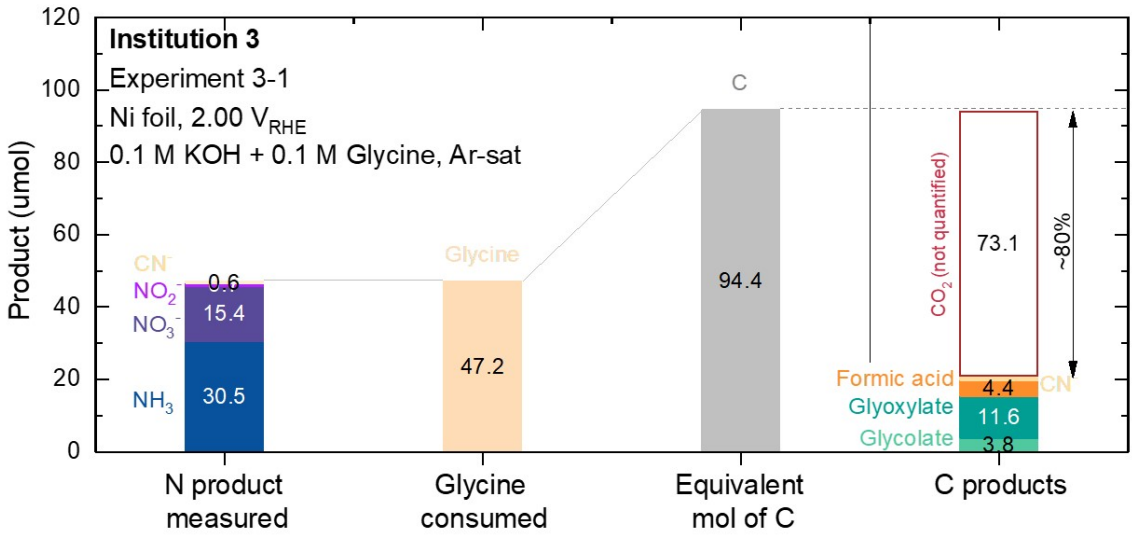

Figure S33. Carbon balance accounting from electrochemical glycine oxidation on Ni foil at 2.00 V_{RHE} from experiment 3-1 (see **Figures S23** and **Table S1**). The first bar showed the sum of nitrogen products (NH_3, NO_3^- and NO_2^-) experimentally quantified via H-NMR and ion chromatography. The second bar shows the equivalent glycine consumed during electrolysis, calculated based on the conservation of N atoms since each glycine molecule (NH_2CH_2COOH) possesses one N atom. The third bar shows the equivalent mol of carbon based on the conservation of C atoms, as each glycine molecule constitutes two C atoms. The final bar represents the carbon products quantified via ion chromatography (see **Figure S13**), which amount to ~20% of the carbon equivalents of consumed glycine. The corresponding carbon faradaic efficiencies were shown in **Figure 3** of the main text. The remaining unclosed carbon balance (~80%) likely corresponds to CO_2 (remaining as CO_3^{2-} in the alkaline electrolyte) which were not quantified for the particular experiment but is consistent with the ~80% carbon balance from CO_2 quantified in experiment 1-1 shown in **Figure S32**.

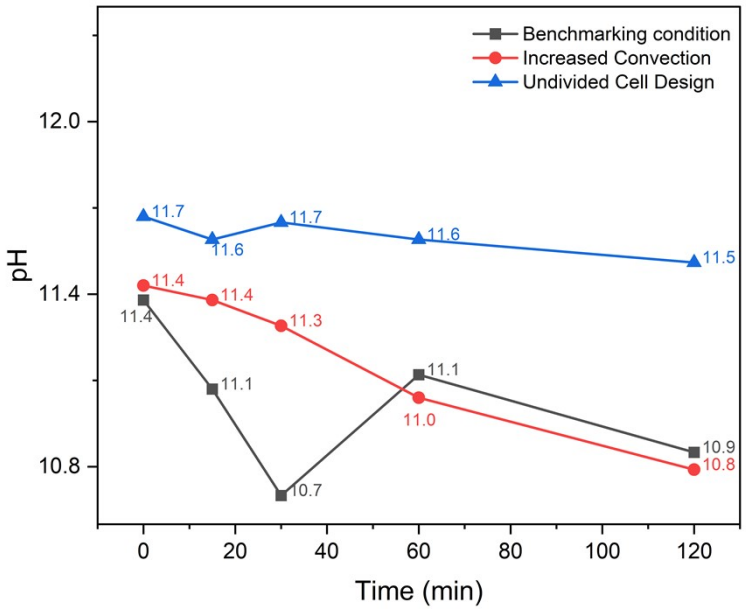

Figure S34. pH measurement of the glycine solution during electrochemical oxidation in different configurations. Experiments at benchmarking conditions and increased convection were run in a divided cell. The pH in these experiments show a much steeper decline compared to the experiment in the single-compartment (i.e. undivided) cell.

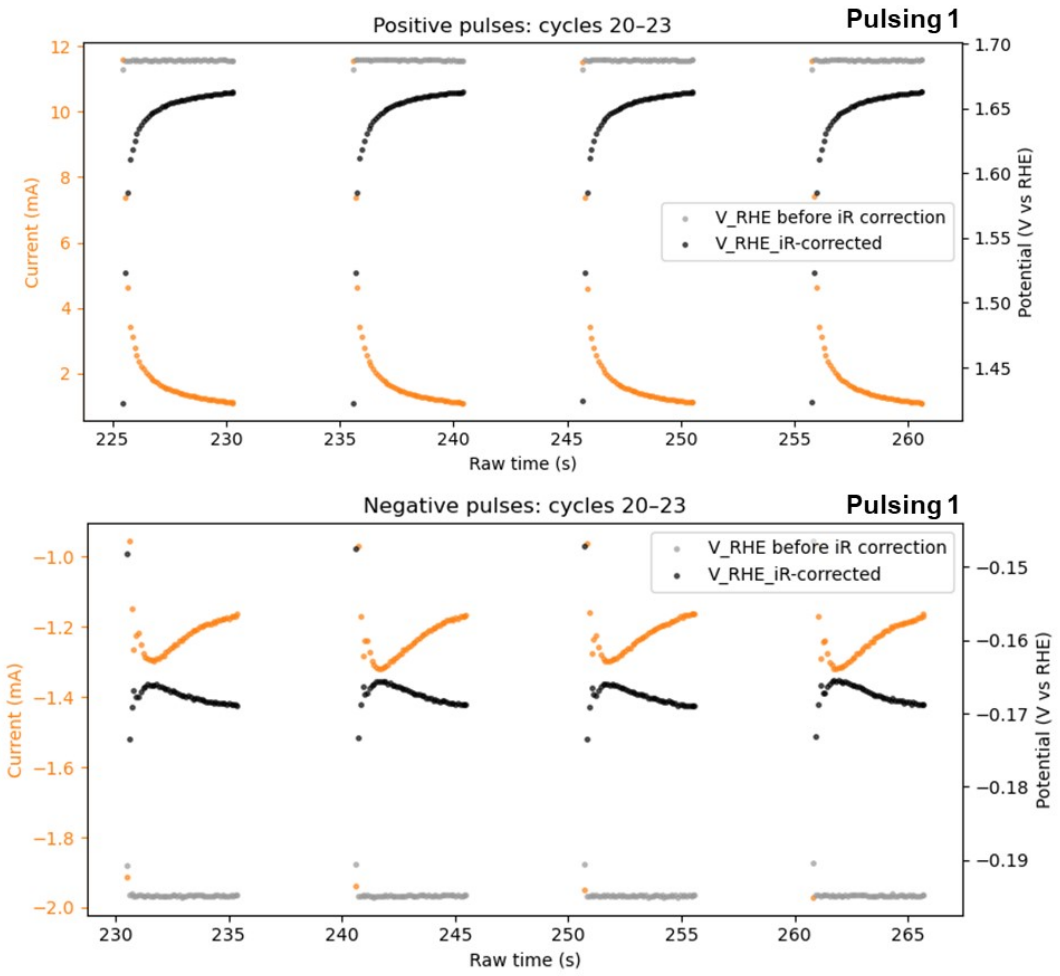

Figure S35. Representative zoomed-in chronoamperometry profile during the 'Pulsing 1' (lowest positive potential) experiment. Top and bottom panels show the positive and negative pulses, respectively. Greater fluctuations in the iR-corrected potential were observed compared to the constant potential experiment due to variations in the current during the 5 second pulse.

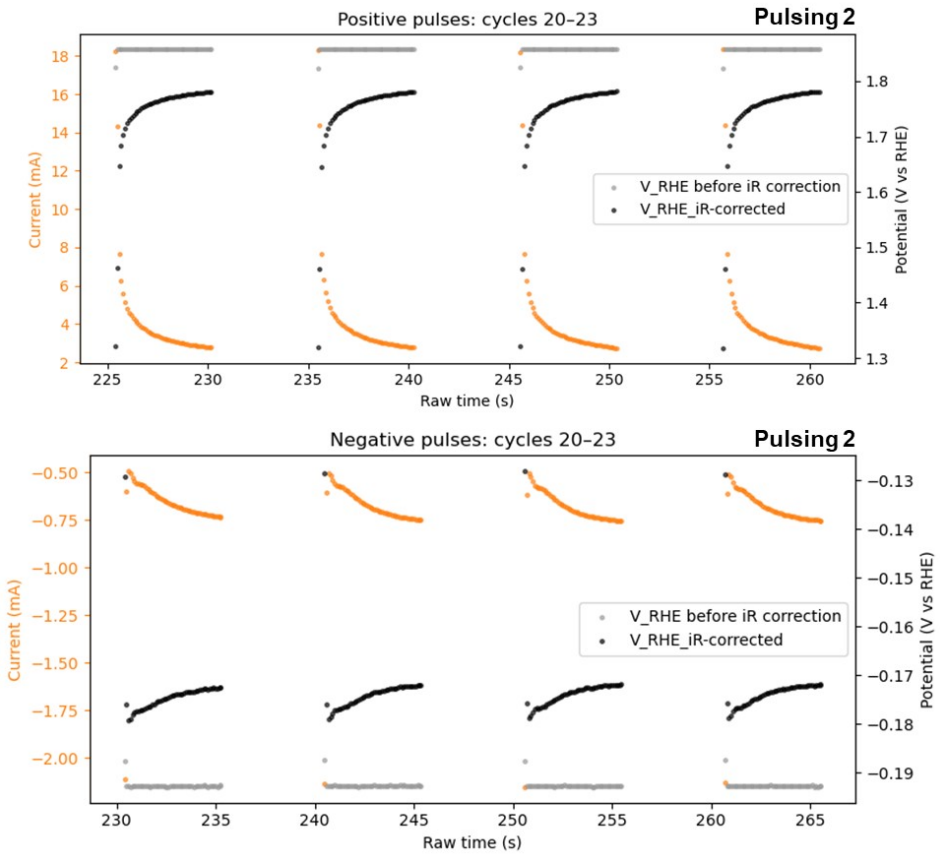

Figure S36. Representative zoomed-in chronoamperometry profile during the 'Pulsing 2' (moderate positive potential) experiment. Top and bottom panels show the positive and negative pulses, respectively. Greater fluctuations in the iR-corrected potential were observed compared to the constant potential experiment due to variations in the current during the 5 second pulse.

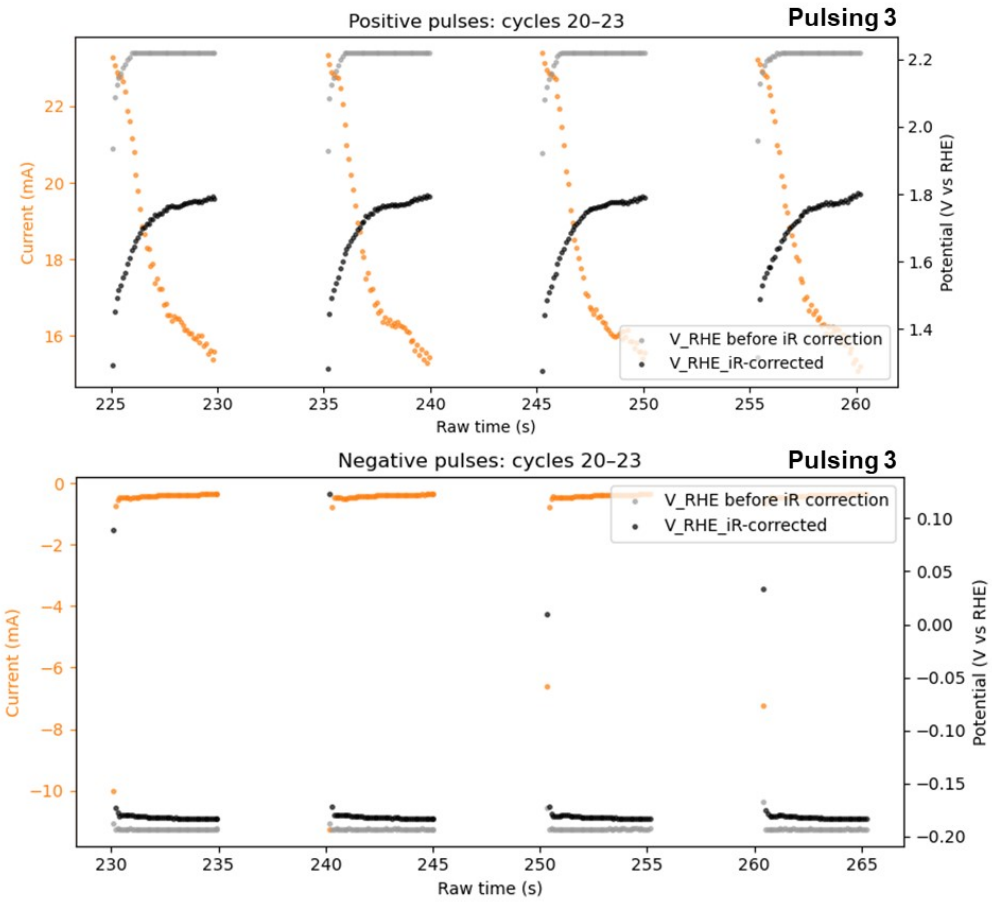

Figure S37. Representative zoomed-in chronoamperometry profile during the 'Pulsing 3' (highest positive potential) experiment. Top and bottom panels show the positive and negative pulses, respectively. Greater fluctuations in the iR-corrected potential were observed compared to the constant potential experiment due to variations in the current during the 5 second pulse.

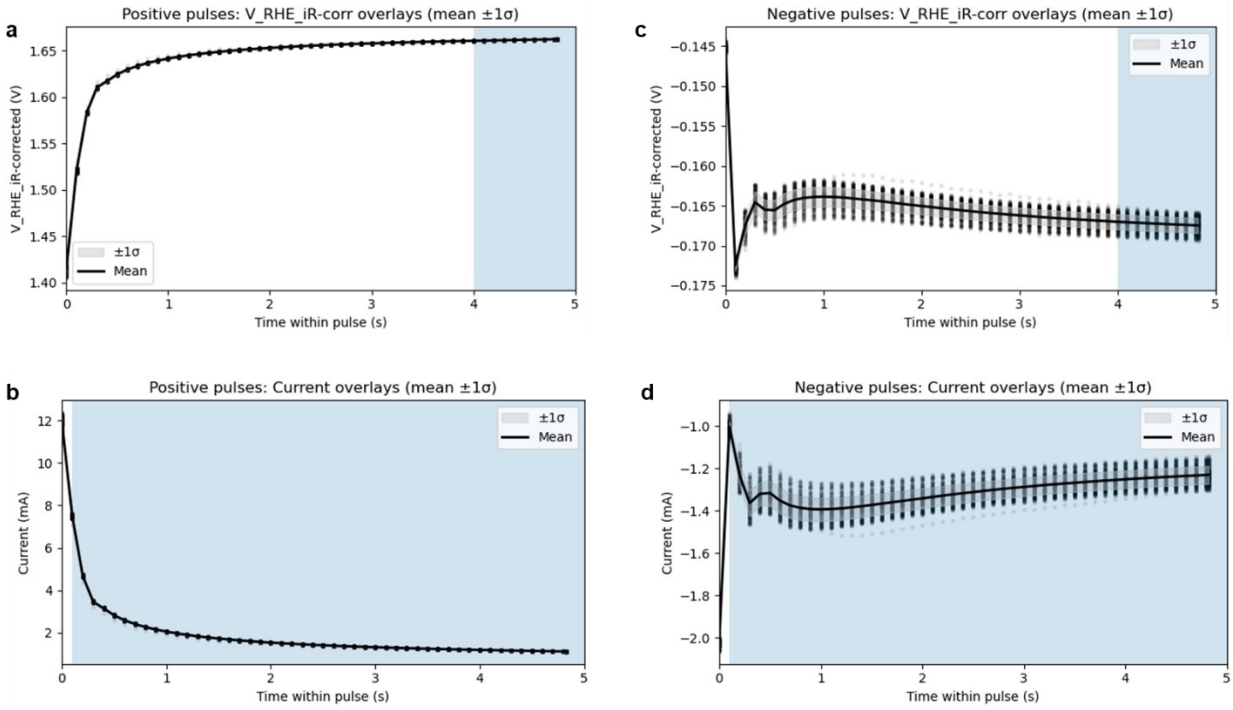

Figure S38. Processing of electrochemical data for 'Pulsing 1' experiment (lowest positive potential). Overlay of the iR-corrected potential on the RHE scale (a) and the current (b) across all of the 5 second positive pulses. The region shaded in blue in (a) corresponds to the final 1 second over which the working electrode potential is calculated and reported in **Figure 5b**. The shaded region in panel (b) indicates the region over which the current is integrated to obtain charge passed during electrolysis. The first 0.1 s has been excluded to remove the contribution from non-faradaic (i.e. capacitive) currents. The same plot and analyses for the negative pulses are shown in panels (c) and (d).

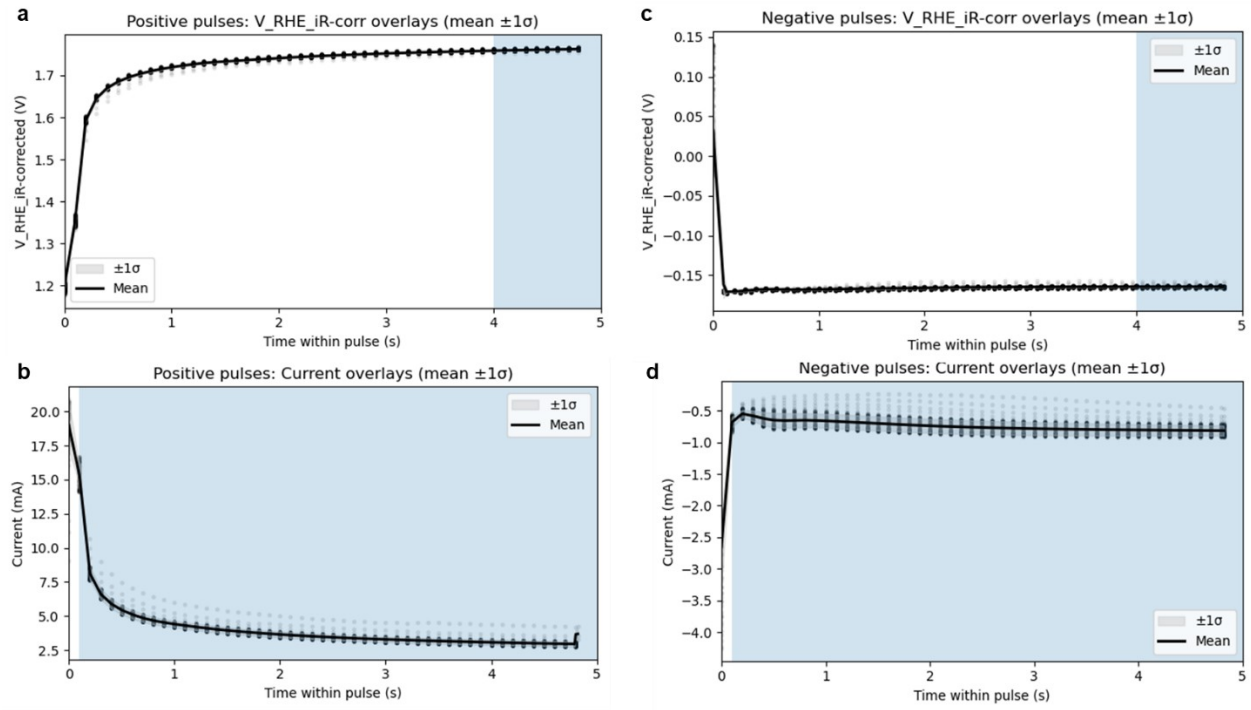

Figure S39. Processing of electrochemical data for 'Pulsing 2' experiment (moderate positive potential). Overlay of the iR-corrected potential on the RHE scale (a) and the current (b) across all of the 5 second positive pulses. The region shaded in blue in (a) corresponds to the final 1 second over which the working electrode potential is calculated and reported in **Figure 5c**. The shaded region in panel (b) indicates the region over which the current is integrated to obtain charge passed during electrolysis. The first 0.1 s has been excluded to remove the contribution from non-faradaic (i.e. capacitive) currents. The same plot and analyses for the negative pulses are shown in panels (c) and (d).

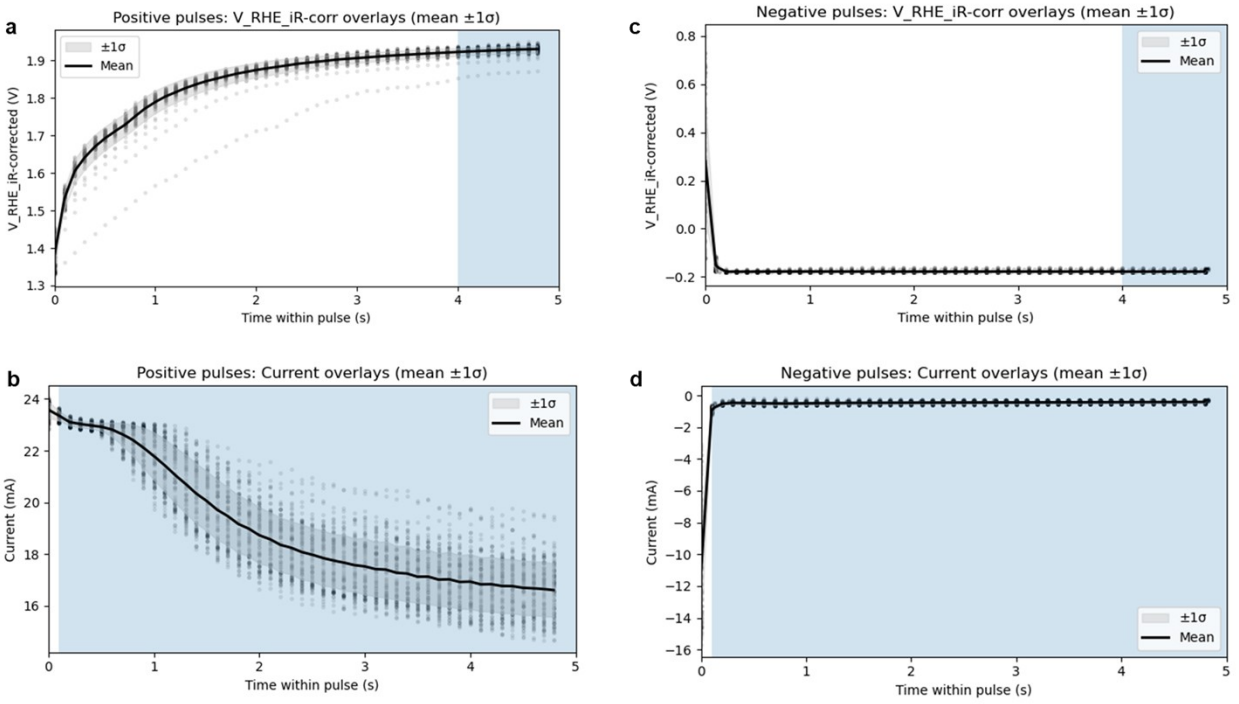

Figure S40. Processing of electrochemical data for 'Pulsing 3' experiment (highest positive potential). Overlay of the iR-corrected potential on the RHE scale (a) and the current (b) across all of the 5 second positive pulses. The region shaded in blue in (a) corresponds to the final 1 second over which the working electrode potential is calculated and reported in **Figure 5d**. The shaded region in panel (b) indicates the region over which the current is integrated to obtain charge passed during electrolysis. The first 0.1 s has been excluded to remove the contribution from non-faradaic (i.e. capacitive) currents. The same plot and analyses for the negative pulses are shown in panels (c) and (d).

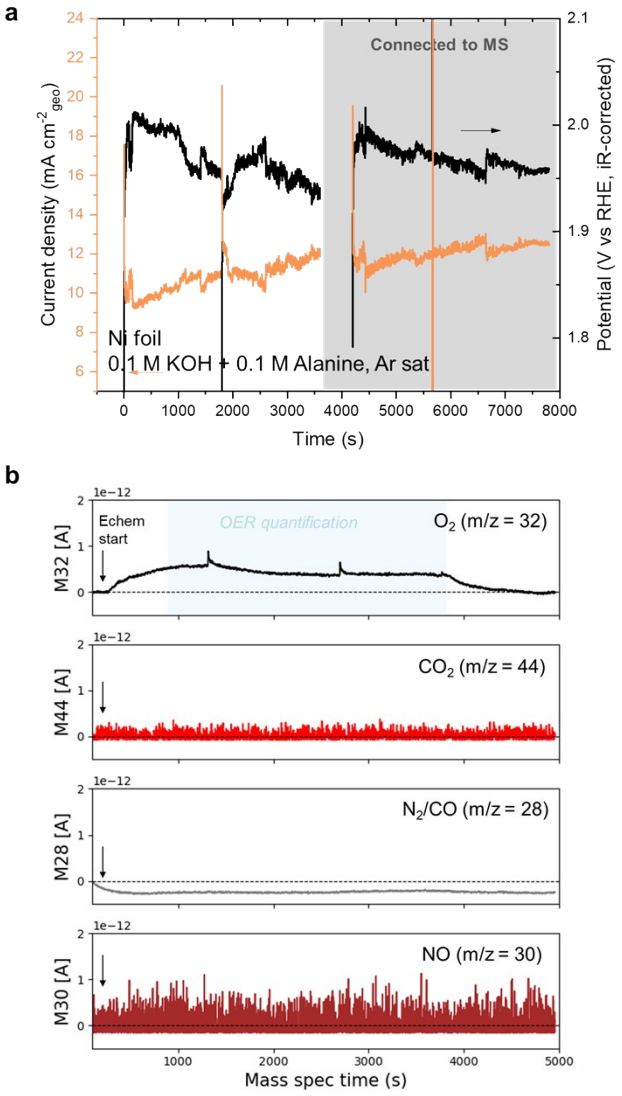

Figure S41. (a) Chronoamperometry profiles of electrochemical oxidation of 0.1 M Alanine on Ni foil electrode at 2.00 V_{RHE} over 2 hours. Equations-based RHE conversion with iR correction was done by utilizing the solution pH (see Supplementary Note 2), where the pH for 0.1 M KOH + 0.1 M Alanine was measured at 10.7 ± 0.1. The region shaded in grey corresponds to the period when the H-cell was connected to the mass spectrometer in the manner described in **Figure S11**. The corresponding mass spectrometer signal is shown in panel (b), where the spectra at m/z = 32, 44, 28 and 30 have been background-subtracted by the baseline signal, defined as the average of the signal before the start of electrochemical program over a period 120 s. Only O_2 (m/z = 32) was observed during glycine oxidation. To obtain O_2 Faradaic efficiency, O_2 was quantified by averaging the mass spectrometer signal over the period shaded in blue i.e. when the mass spectrometer signal has been stabilized and be converted it to O_2 production rate using the calibration curve established in Panel c of **Figure S12**.

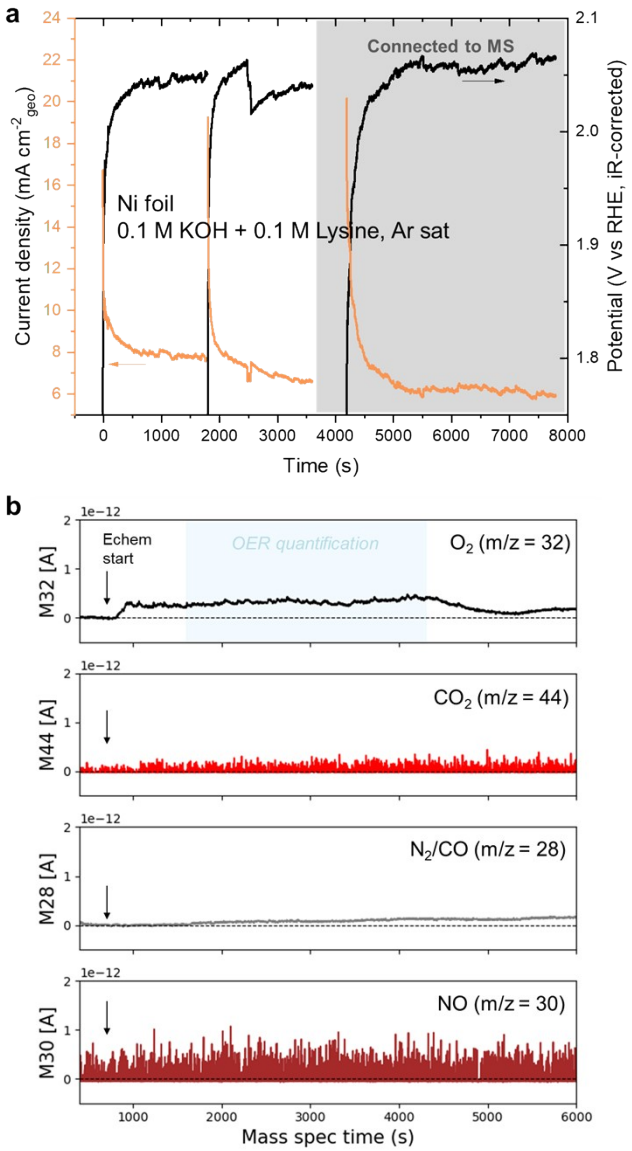

Figure S42. (a) Chronoamperometry profiles of electrochemical oxidation of Lysine on Ni foil electrode at 2.00 V_{RHE} over 2 hours. Equations-based RHE conversion with iR correction was done by utilizing the solution pH (see Supplementary Note 2), where the pH for 0.1 M KOH + 0.1 M Lysine was measured at 11.6 ± 0.1. The region shaded in grey corresponds to the period when the H-cell was connected to the mass spectrometer in the manner described in **Figure S11**. The corresponding mass spectrometer signal is shown in panel (b), where the spectra at m/z = 32, 44, 28 and 30 have been background-subtracted by the baseline signal, defined as the average of the signal before the start of electrochemical program over a period 120 s. Only O_2 (m/z = 32) was observed during glycine oxidation. To obtain O_2 faradaic efficiency, O_2 was quantified by averaging the mass spectrometer signal over the period shaded in blue i.e. when the mass spectrometer signal has been stabilized and been converted it to O_2 production rate using the calibration curve established in Panel c of **Figure S12**.

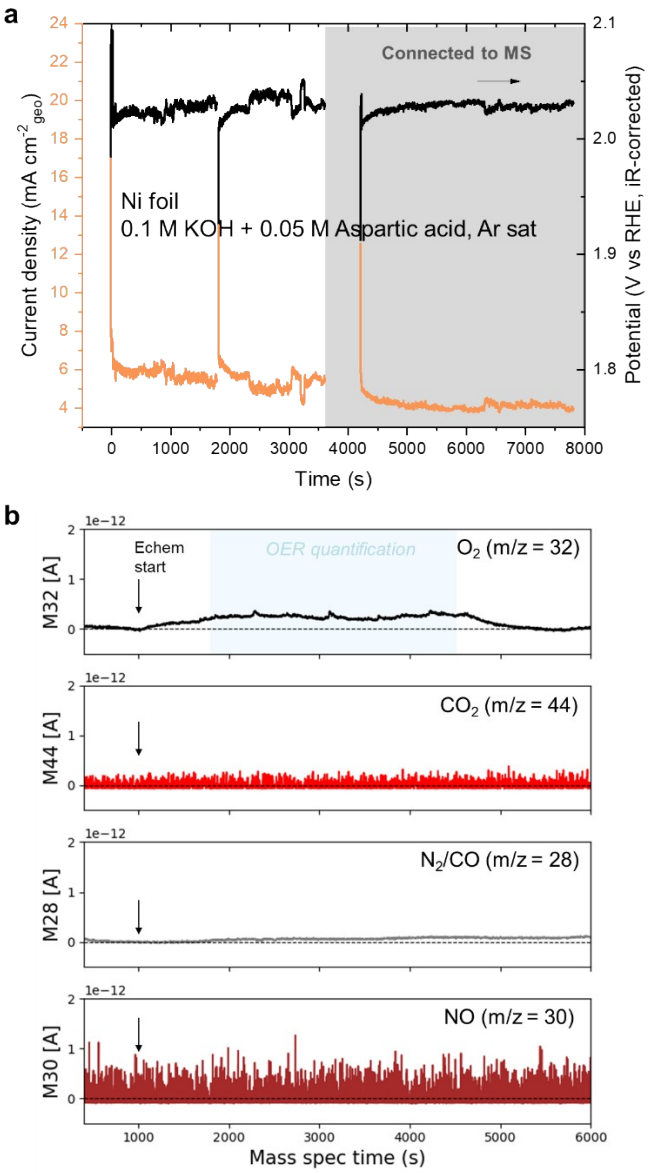

Figure S43. (a) Chronoamperometry profiles of electrochemical oxidation of Lysine on Ni foil electrode at 2.00 V_{RHE} over 2 hours. Equations-based RHE conversion with iR correction was done by utilizing the solution pH (see Supplementary Note 2), where the pH for 0.1 M KOH + 0.05 M Aspartic acid was measured at 10.4 ± 0.1. The region shaded in grey corresponds to the period when the H-cell was connected to the mass spectrometer in the manner described in **Figure S11**. The corresponding mass spectrometer signal is shown in panel (b), where the spectra at m/z = 32, 44, 28 and 30 have been background-subtracted by the baseline signal, defined as the average of the signal before the start of electrochemical program over a period 120 s. Only O_2 (m/z = 32) was observed during glycine oxidation. To obtain O_2 faradaic efficiency, O_2 was quantified by averaging the mass spectrometer signal over the period shaded in blue i.e. when the mass spectrometer signal has been stabilized and been converted it to O_2 production rate using the calibration curve established in Panel c of **Figure S12**.

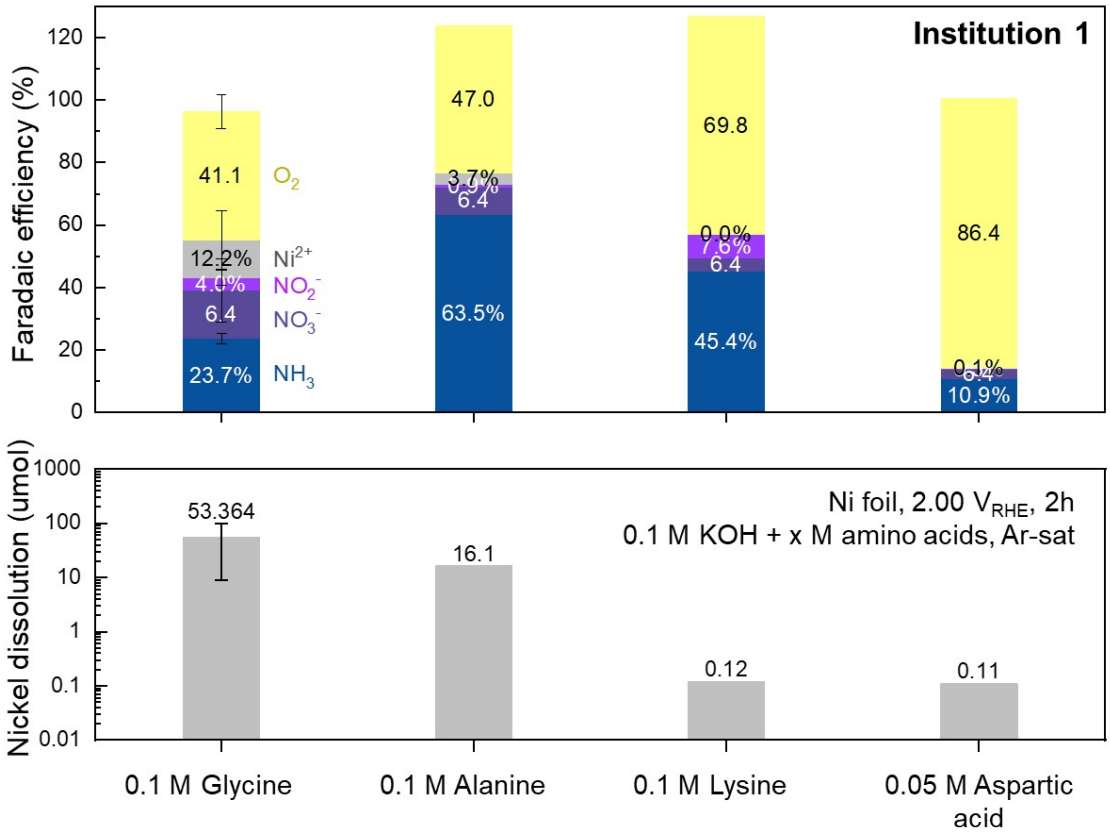

Figure S44. Faradaic efficiency (top) and the Ni dissolution quantified via ICP-MS (bottom) of electrochemical oxidation of various amino acids in alkaline electrolyte using Ni foil at 2.00 V_{RHE} over 2 hours in an H-cell. The glycine datapoints correspond to the 'benchmarking' condition displayed throughout the manuscript, where the error bars correspond to the standard deviation over up to n=7 independent trials (see **Figure S22**). A concentration of 0.05 M Aspartic acid has been chosen in order to maintain an alkaline pH enabling cross-amino acid comparisons over Ni electrode, where the pH of 0.1 M KOH + 0.1 M Aspartic acid was measured to be ~4.5 while 0.1 M KOH + 0.05 M Aspartic acid was 10.4 (see **Supplementary Note 2**). The chronoamperometry profiles and gas-phase characterization for the other amino acids can be found in **Figures S41-S43**. To enable the Faradaic efficiency calculations, the generation of N products are assumed to be accompanied by complete C oxidation to CO_2, where details of the number of electrons (z_{e^-}) can be found in **Table S1**. Therefore, the Faradaic efficiency values for NH_3, NO_3^- and NO_2^- served as an upper bound. We note that the cumulative faradaic efficiency for Alanine and Lysine, both at ~125% appeared to exceed unity, which points to the possibility of incomplete oxidation of the carbon and hence an overestimate in the z_{e^-} values.

Table S1. Summary of electrochemical glycine oxidation results in the three institutions. The average potential on the RHE scale is provided after iR correction. For Institution 1, the averaged faradaic efficiencies are calculated across the 2 hour tests between 1-1 and 1-7.

							Faradaic efficiency (%)			
	Avg potential (V_{RHE})	Q (C)	NH_3 (umol)	NO_3^- (umol)	NO_2^- (umol)	Ni^{2+} (umol)	NH_3	NO_3^-	NO_2^-	Ni^{2+}
Institution 1										
1-1	2.00 ± 0.016	132.2	57.7	13.2	10.8	176.7	25.3 %	13.5 %	9.4%	25.8 %
1-2	2.02 ± 0.069	92.9	36.5	13.7	4.3	-	22.7 %	19.9 %	5.3%	-
1-3	2.04 ± 0.041	108.7	44.9	14.2	4.1	-	23.9 %	17.7 %	4.3%	-
1-4 (2 h)	2.00 ± 0.025	61.6	28.5	-	-	-	23.5 %	-	-	-
1-4 (1 h)		29.1	11.8	-	-	-	18.0 %	-	-	-
1-5 (2 h)	1.99 ± 0.021	65.9	26.6	-	-	-	23.4 %	-	-	-
1-5 (1 h)		31.0	10.9	-	-	-	20.4 %	-	-	-
1-6	1.99 ± 0.016	72.74	27.7	9.1	2.6	0.69	22.0 %	17.0 %	4.1 %	0.2 %
1-7	2.03 ± 0.013	57.0	21.6	3.6	1.6	0.40	22.0 %	8.5 %	3.2 %	0.1 %
13C2-glycine	2.01 ± 0.017	76.0	29.3	-	-	333.8	22.3 %	0.0%	0.0%	84.7 %*
15N2-glycine	2.01 ± 0.046	108.6	35.6	-	-	74.9	19.0 %	0.0%	0.0%	13.3 %
						Average	23.6 %	16.6 %	10.2 %	18.0 %
						Standard deviation	1.1%	5.7%	3.9%	31.0 %
Institution 2										
2-1	2.01 ± 0.037	42.7	35.5	6.7	7.9	0.0	23.8 %	10.4 %	10.6 %	-
2-2	1.99 ± 0.043	81.4	35.1	11.3	7.7	0.0	25.0 %	18.8 %	11.0 %	-
2-3	1.98 ± 0.027	68.3	26.3	11.9	8.4	106.8	22.3 %	23.5 %	14.2 %	30.2 %
2-4	2.00 ± 0.013	121.2	48.6	12.3	5.1	28.3	23.2 %	13.7 %	4.9%	4.5%
						Average	23.6 %	16.6 %	10.2 %	17.3
						Standard deviation	1.1%	5.7%	3.9%	18.1
Institution 3										
3-1	2.03 ± 0.02	65.8	30.5	15.4	0.7	9.3	26.8 %	31.5 %	1.2%	2.7%
3-2	1.99 ± 0.033	79.5	25.5	20.9	5.1	0.0	18.5 %	35.6 %	7.4%	0.0%
						Average	22.7 %	33.6 %	4.3%	1.4%
						Standard deviation	5.9%	2.8%	4.4%	1.9%
						Cross-institution average	23.3 % [a]	21.9 % [b]	6.4 % [c]	12.2 % [d]

				Cross-institution standard deviation			0.6 %	10.1 %[b]	3.2 %[c]	11.4 %[d]
Additional experiments – Institution 3										
Larger convection	2.04 ± 0.03	92.2	27.9	11.0	8.6	0.5	17.5 %	16.1 %	10.7 %	0.1%
Larger electrode	2.04 ± 0.03	88.5	61.9	7.3	0.7	3.8	40.5 %	11.2 %	0.9%	0.8%
Single cell	2.03 ± 0.05	101.3	30.0	35.2	1.8	3.2	17.2 %	46.9 %	2.0%	0.6%
Additional experiments – Institution 1										
Alanine	1.98 ± 0.025	82.2	45.1	3.7	0.4	16.1	63.5 % [e]	8.6 % [f]	0.9 % [g]	3.7 % [d]
Lysine	2.04 ± 0.030	51.9	17.1	0.99	2.0	0.12	45.4 % [h]	4.0 % [i]	7.6 % [j]	0.04 % [d]
Lysine – trial 2	1.99 ± 0.028	54.9	16.9				41.5 %[h]			
Aspartic Acid	2.03 ± 0.007	35.2	3.3	0.53	0.06	0.11	10.9 % [k]	2.9 % [l]	0.3 % [m]	0.06 % [d]

***** denotes data points excluded from the statistical analysis

[a] Glycine/NH_3 FE calculation is based on n_{e^-} = 6 from $NH_2CH_2COOH + 2H_2O \rightarrow NH_3 + 2CO_2 + 6H^+ + 6e^-$

[b] Glycine/NO_3^- FE calculation is based on n_{e^-} = 14 from $NH_2CH_2COOH + 5H_2O \rightarrow NO_3^- + 2CO_2 + 15H^+ + 14e^-$

[c] Glycine/NO_2^- FE calculation is based on n_{e^-} = 12 from $NH_2CH_2COOH + 4H_2O \rightarrow NO_2^- + 2CO_2 + 13H^+ + 12e^-$

[d] Ni corrosion FE calculation is based on ne- = 2 from $Ni \rightarrow Ni^{2+} + 2e^-$

[e] Alanine/NH_3 FE calculation is based on n_{e^-} = 12 from $NH_2CH(CH)_3COOH + 4H_2O \rightarrow NH_3 + 3CO_2 + 12H^+ + 12e^-$

[f] Alanine/NO_3^- FE calculation is based on n_{e^-} = 20 from $NH_2CH(CH)_3COOH + 7H_2O \rightarrow NO_3^- + 3CO_2 + 21H^+ + 20e^-$

[g] Alanine/NO_2^- FE calculation is based on n_{e^-} = 18 from $NH_2CH(CH)_3COOH + 6H_2O \rightarrow NO_2^- + 3CO_2 + 19H^+ + 18e^-$

[h] Lysine/NH_3 FE calculation is based on n_{e^-} = 14 from $0.5NH_2(CH_2)_4CH(NH_2)COOH + 5H_2O \rightarrow NH_3 + 3CO_2 + 14H^+ + 14e^-$

[i] Lysine/NO_3^- FE calculation is based on n_{e^-} = 22 from $0.5NH_2(CH_2)_4CH(NH_2)COOH + 8H_2O \rightarrow NO_3^- + 3CO_2 + 23H^+ + 22e^-$

[j] Lysine/NO_2^- FE calculation is based on n_{e^-} = 20 from $0.5NH_2(CH_2)_4CH(NH_2)COOH + 7H_2O \rightarrow NO_2^- + 3CO_2 + 21H^+ + 20e^-$

[k] Aspartic acid/NH_3 FE calculation is based on n_{e^-} = 12 from $NH_2CH(CH_2COOH)COOH + 4H_2O \rightarrow NH_3 + 4CO_2 + 12H^+ + 12e^-$

[l] Aspartic /NO_3^- FE calculation is based on n_{e^-} = 20 from $NH_2CH(CH_2COOH)COOH + 7H_2O \rightarrow NO_3^- + 4CO_2 + 21H^+ + 20e^-$

[m] Aspartic/NO_2^- FE calculation is based on n_{e^-} = 18 from $NH_2CH(CH_2COOH)COOH + 4H_2O \rightarrow NO_2^- + 2CO_2 + 19H^+ + 18e^-$

Table S2. Summary of the thermodynamic calculations used to determine standard reduction potentials, including Gibbs free energy values, electron stoichiometry, and conversion to the SHE scale by assuming the equilibrium between $2(H^+ + e^-) \leftrightharpoons H_2$. The formula-embedded workbook for the thermodynamic calculations can be found in the enclosed link*

[R]			**[O]**			**ΔG_r^0**	**n_{e^-}**	**E^0 (SHE)**
Glycine to ammonia and CO_2								
NH_2CH_2COOH	$+ 2H_2O$		$NH_{3(g)}$	$+ 2CO_2$	+ 6 (H+ + e-)	-37.53	6	0.064829
Glycine to nitrate and CO2								
NH_2CH_2COOH	$+ 5H_2O$		$H^+NO_3^-$ (aq)	$2CO_2$	+ 14 (H+ + e-)	-654.117	14	0.484248
Glycine to nitrite and CO_2								
NH_2CH_2COOH	$+ 4H_2O$		$H^+NO_2^-$ (aq)	$2CO_2$	+ 12 (H+ + e-)	-496.038	12	0.428424
Ammonia to nitrate								
NH_3	$+ 3H_2O$		$H^+NO_3^-$ (aq)		+ 8 (H+ + e-)	-616.587	8	0.798812
Glycine to formaldehyde and CO_2 and NH_3								
NH_2CH_2COOH	$+ H_2O$		NH_3	$CH_2O + CO_2$	+ 2 (H+ + e-)	-92.09	2	0.47724

*Interactive workbook:
https://www.dropbox.com/scl/fi/hwc700r90vst9igh23vbl/Thermodynamics_workbook.xlsx?rlkey=8tfr3pvv958l1bdu6shvrcn7i&st=kmspj86t&dl=0

Table S3. Calculation of the Gibbs free energy of reaction for various carbon–nitrogen compounds and intermediates relevant to glycine oxidation. C, N, H, and O are referenced to CO_2(g), N_2(g), H_2(g) (all at 1 bar), and H_2O(l), respectively, with reactions balanced to ensure stoichiometric consistency. Glycine, glyoxylic acid, and glycolic acid are considered in the crystalline phase; methylamine, formaldehyde and ammonia in the gas phase; and cyanic acid, formic acid, and acetic acid in the liquid phase. Thermodynamic data are taken from the NBS thermodynamic database. For glyoxylic acid (in its hydrated form, dihydroxyacetic acid) and glycolic acid, only standard enthalpies of formation are available. Their Gibbs free energies of formation were therefore estimated by assuming the same TΔS term as for glycine. The formula-embedded workbook for the thermodynamic calculations can be found in the enclosed link*

Alpha carbon oxidation state	Species	Equation	ΔG^o_r (kJ mol^{-1})
-3	Acetic acid	$CH_3COOH + 2H_2O$ <- $2CO_2 + 8H_2$	-75.44
-1	Glycolic acid	$CH_2OHCOOH + H_2O$ <- $2CO_2 + 6H_2$	47.249
-1	Glycine	$NH_2CH_2COOH + 2H_2O$ <- $2CO_2 + 0.5N_2 + 9H_2$	-53.98
1	Glyoxylic acid	$CH(OH)_2COOH$ <- $2CO_2 + 4H_2$	112.878
2	Formic acid	$HCOOH$ <- $CO_2 + 2H_2$	33.01
-1	Glycine (from ammonia)	$NH_2CH_2COOH + 2H_2O$ <- $2CO_2 + NH_3 + 6\ H_2$	-37.53
4	CO_2 and NH_3	NH3 <- $0.5N_2 + 3\ H_2$	-16.45
Alpha carbon oxidation state	Species		
-1	Glycine	$NH_2CH_2COOH + 2H_2O$ <- $2CO_2 + 0.5N_2 + 9\ H_2$	-53.98
-2	methylamine	$2CH_3NH_2 + 4H_2O$ <- $2CO_2 + N_2 + 16\ H_2$	-95.478
0	formaldehyde	$HCHO + H_2O$ <- $CO_2 + 4\ H_2$	54.56
2	Cyanide	$HCN + 2H_2O$ <- $CO_2 + 0.5N_2 + 5\ H_2$	45.071
0	Formaldehyde, NH_3	$HCHO + NH_3 + H_2O$ <- $CO_2 + 0.5N_2 + 7\ H_2$	38.11
4	CO_2 and NH_3	NH_3 <- $0.5N_2 + 3\ H_2$	-16.45
2	Formic acid	$HCOOH$ <- $CO_2 + 2\ H_2$	33.01

*Interactive workbook:
https://www.dropbox.com/scl/fi/hwc700r90vst9igh23vbl/Thermodynamics_workbook.xlsx?rlkey=8tfr3pvv958l1bdu6shvrcn7i&st=kmspj86t&dl=0

Table S4. pH behavior of glycine solution during electrochemical oxidation. Both experiments at benchmarking conditions and increased convection were run in an H-cell cell. The pH in these experiments show a much steeper decline compared to the experiment in the undivided cell.

	pH		
Time(min)	Benchmarking Condition	Increased Convection	Undivided Cell
0	11.4	11.4	11.7
15	11.1	11.4	11.6
30	10.7	11.3	11.7
60	11.1	11	11.6
120	10.9	10.8	11.5

Table S5. Summary of average potentials and charge passed in the positive and negative pulses during the pulsing experiments. P1, P2 and P3 correspond to 'Pulsing 1' (lowest positive potential), 'Pulsing 2' (moderate positive potential) and 'Pulsing 3' (highest positive potential), respectively. The positive and negative potentials are averaged from the last 1 second from all of the 5 s pulses during the 1 h experiment, as demonstrated in **Figure S38-40**. The positive and negative charges are calculated excluding the first 0.1 s to exclude capacitive charge, as demonstrated in **Figure S35-S37**.

	Positive pulse (V_{RHE})	Negative pulse (V_{RHE})	Average Positive potential (V_{RHE})	Stdev Positive potential (V_{RHE})	Average Negative potential (V_{RHE})	Stdev Negative potential (V_{RHE})	Q_+ (C)	Q_- (C)	Q_+ average (C)	Q_- average (C)
1-P3(1)	1.752	-0.175					31.9	-1.0		
1-P3(2)	1.882	-0.180	1.828	0.067	-0.190	0.021	29.6	-1.2	30.4	-1.1
1-P3(3)	1.851	-0.214					29.8	-1.1		
1-P1(1)	1.652	-0.162					1.9	-2.9		
1-P1(2)	1.663	-0.168	1.660	0.007	-0.162	0.007	3.8	-2.7	2.8	-2.3
1-P1(3)	1.664	-0.155					2.8	-1.4		
1-P1(4)	1.663	-0.165					2.6	-2.2		
1-P2(1)	1.768	-0.167					6.9	-1.5		
1-P2(2)	1.792	-0.174	1.787	0.017	-0.175	0.008	6.1	-1.4	6.3	-1.3
1-P2(3)	1.801	-0.184					5.8	-0.9		

Table S6. Summary of faradaic efficiencies from pulsing experiments with respect to the three accounting methods. Highlighted cells indicate unphysical values where the positive charge passed is less than negative (due to the overall low charge passed, see **Table S5**) and therefore excluded from the Faradaic efficiency calculation.

Accounting 1: Total charge passed										
	Pulsing 3 - most positive			Pulsing 1 - lowest positive				Pulsing 2 - moderate positive		
FE	1-P3(1)	1-P3(2)	1-P3(3)	1-P1(1)	1-P1(2)	1-P1(3)	1-P1(4)	1-P2(1)	1-P2(2)	1-P2(3)
15min	16.1%	17.2%	9.4%	-114.2%	259.6%	65.7%	358.0%	46.6%	43.8%	49.8%
30min	14.9%	20.0%	11.9%	-157.5%	108.1%	76.4%	288.2%	36.7%	46.0%	42.2%
1h	14.9%	21.7%	14.0%	-135.4%	81.0%	76.2%	221.7%	36.2%	45.3%	40.7%
Average FE @ 1h	16.9%			78.6%				40.7%		
Stdev	4.2%			3.4%				4.6%		
Accounting 2: Positive charge only										
	Pulsing 3 - most positive			Pulsing 1 - lowest positive				Pulsing 2 - moderate positive		
FE	1-P3(1)	1-P3(2)	1-P3(3)	1-P1(1)	1-P1(2)	1-P1(3)	1-P1(4)	1-P2(1)	1-P2(2)	1-P2(3)
15min	15.7%	16.3%	9.3%	62.3%	72.4%	33.3%	70.0%	37.4%	35.6%	46.1%
30min	14.5%	19.1%	11.5%	87.2%	32.7%	34.4%	50.1%	29.1%	36.1%	37.6%
1h	14.5%	20.8%	13.5%	72.2%	23.0%	37.0%	29.9%	36.2%	34.6%	34.5%
Average FE @ 1h	16.3%			40.5%				35.1%		
Stdev	4.0%			21.9%				0.9%		
Accounting 3: Total absolute charge										
	Pulsing 3 - most positive			Pulsing 1 - lowest positive				Pulsing 2 - moderate positive		
FE	1-P3(1)	1-P3(2)	1-P3(3)	1-P1(1)	1-P1(2)	1-P1(3)	1-P1(4)	1-P2(1)	1-P2(2)	1-P2(3)
15min	15.4%	15.6%	9.2%	24.5%	42.1%	22.3%	38.8%	31.2%	30.0%	43.0%
30min	14.1%	18.4%	11.3%	34.2%	19.2%	22.2%	27.4%	24.1%	29.8%	34.0%
1h	14.0%	20.0%	13.0%	28.5%	13.4%	24.4%	16.0%	23.3%	28.0%	30.0%
Average FE @ 1h	15.7%			20.6%				27.1%		
Stdev	3.8%			7.1%				3.4%		

References

(1) Wei, C.; Rao, R. R.; Peng, J.; Huang, B.; Stephens, I. E. L.; Risch, M.; Xu, Z. J.; Shao-Horn, Y. Recommended Practices and Benchmark Activity for Hydrogen and Oxygen Electrocatalysis in Water Splitting and Fuel Cells. *Adv. Mater.* **2019**, *31* (31), 1806296. https://doi.org/10.1002/adma.201806296.

(2) Marangoni, D. G.; Smith, R. S.; Roscoe, S. G. Surface Electrochemistry of the Oxidation of Glycine at Pt. *Can. J. Chem.* **1989**, *67* (5), 921–926. https://doi.org/10.1139/v89-141.

(3) Huerta, F.; Morallón, E.; Cases, F.; Rodes, A.; Vázquez, J. L.; Aldaz, A. Electrochemical Behaviour of Amino Acids on Pt(*h*,*k*,*l*): A Voltammetric and in Situ FTIR Study. Part 1. Glycine on Pt(111). *J. Electroanal. Chem.* **1997**, *421* (1), 179–185. https://doi.org/10.1016/S0022-0728(96)04820-6.